Rate-Splitting Multiple Access for Satellite-Terrestrial Integrated Networks: Benefits of Coordination and Cooperation

Longfei Yin and Bruno Clerckx, *Fellow, IEEE*

***Abstract*— This paper investigates the joint beamforming design problem to achieve max-min rate fairness in a satellite-terrestrial integrated network (STIN) where the satellite provides wide coverage to multibeam multicast satellite users (SUs), and the terrestrial base station (BS) serves multiple cellular users (CUs) in a densely populated area. Both the satellite and BS operate in the same frequency band. Since rate-splitting multiple access (RSMA) has recently emerged as a promising strategy for non-orthogonal transmission and robust interference management in multi-antenna wireless networks, we present two RSMA-based STIN schemes, namely the coordinated scheme relying on channel state information (CSI) sharing and the cooperative scheme relying on CSI and data sharing. Our objective is to maximize the minimum fairness rate amongst all SUs and CUs subject to transmit power constraints at the satellite and the BS. A joint beamforming algorithm is proposed to reformulate the original problem into an approximately equivalent convex one, which can be iteratively solved. Moreover, an expectation-based robust joint beamforming algorithm is proposed against the practical environment when the satellite channel phase uncertainties are considered. Simulation results demonstrate the effectiveness and robustness of our proposed RSMA schemes for STIN and exhibit significant performance gains compared with various baseline strategies.**

***Index Terms*— Rate-splitting multiple access (RSMA), max-min fairness, satellite-terrestrial integrated network (STIN), beamforming design, multibeam multicast transmission, channel phase uncertainty.**

I. Introduction

In RECENT years, due to the explosive growth of wireless applications and multimedia services, satellite-terrestrial integrated network (STIN) has gained a tremendous amount of attention in both academia and industry as it can provide ubiquitous coverage and convey rich multimedia services, e.g., video on demand (VoD) streaming and TV broadcasting, etc. to users in both densely and sparsely populated areas [1]. The integration of terrestrial and satellite networks is of great potential in achieving geographic coverage, especially for remote areas where no terrestrial base station (BS) infrastructure can be employed [2], [3]. It is envisaged that the C-band ($4-8$ GHz) and S-band ($2-4$ GHz) can be shared between the terrestrial and satellite networks. In addition, Ka band from 20 GHz to 40 GHz is foreseen to be the most promising candidate radio band for the next generation terrestrial cellular networks, and part of this band has already been allocated to the satellite networks [4]. The concept of STIN has been proposed in the literature [5]–[7]. The satellite sub-network shares the same frequency band with the terrestrial sub-network through dynamic spectrum access technology to enhance spectrum utilization, thereby achieving higher spectrum efficiency and throughput. However, aggressive frequency reuse can induce severe interference within and between the sub-networks. In this work, we will concentrate on RSMA-based joint beamforming schemes to efficiently mitigate the interference of STIN.

A. Related Works

A number of research efforts have investigated STIN systems. A coexistence framework of the satellite and terrestrial network was presented in [8]. Transmit beamforming techniques were studied to maximize the signal to interference plus noise ratio (SINR) towards terrestrial users and minimize the interference towards satellite users. Zhu *et al.* [9] studied a time division cooperative STIN, where a weighted max–min fair (MMF) problem was formulated to jointly optimize the beamforming of BSs and the satellite. A multicast beamforming STIN system was investigated in [10] with the aim to maximize the sum of user minimum ratio under constraints of backhaul links and quality of service (QoS). Aforementioned works generally assumed the satellite channels as Rician channels. The effects of satellite antenna gain, path loss and atmospheric attenuation can be taken into account to model more practical satellite channels so as to evaluate the system performance more accurately. In this regard, [4] investigated a joint beamforming scheme for secure communication of STIN

Manuscript received 11 October 2021; revised 5 March 2022 and 21 June 2022; accepted 11 July 2022. Date of publication 28 July 2022; date of current version 9 January 2023. This work was supported in part by the U.K. Engineering and Physical Sciences Research Council (EPSRC) under Grant EP/R511547/1. The associate editor coordinating the review of this article and approving it for publication was M. Wang. *(Corresponding author: Longfei Yin.)*

The authors are with the Communications and Signal Processing Group, Department of Electrical and Electronic Engineering, Imperial College London, London SW7 2AZ, U.K. (e-mail: longfei.yin17@imperial.ac.uk; b.clerckx@imperial.ac.uk).

Color versions of one or more figures in this article are available at https://doi.org/10.1109/TWC.2022.3192980.

Digital Object Identifier 10.1109/TWC.2022.3192980

operating in mmWave frequencies. Lin *et al.* [11] focused on the joint optimization for wireless information and power transfer (WIPT) technique in STINs. In [12], the cache-enabled LEO satellite network was introduced, and the scheme of STIN was proposed to enable an energy-efficient radio access network (RAN) by offloading traffic from BSs through satellite broadcast transmission.

The above works consider conventional space division multiple access (SDMA) based on linear precoding and assume perfect channel state information at the transmitters (CSIT). Each user decodes its desired stream while treating all the other interference streams as noise. The spatial degrees of freedom provided by multiple antennas are exploited, however the effectiveness of beamforming design relies on the accuracy of CSIT significantly. In the real satellite communication (SatCom) environment, one practical issue is that accurate CSI is very difficult to acquire at the gateway (GW) because of the long-distance propagation delay and device mobility. Thus, robust design in the presence of imperfect CSIT has been widely studied in the literature [13]–[18]. References [13]–[15] assumed the satellite channel uncertainty as additive estimation error located in a bounded error region. Robust beamforming was designed based on the optimization of the worst case situation. Yet, due to the special characteristics of satellite channels, the channel magnitude does not vary significantly due to the fact that the channel propagation is dominated by the line-of-sight component. The phase variations constitute the major source of channel uncertainty [19]. Therefore, in [16]–[18], beamforming was studied when considering constant channel amplitudes within the coherence time interval and independent time varying phase components. Considering the phase-blind scenario, the achievable rate performance of RSMA in a MU-MISO network was investigated in [20]. A space-time rate splitting (STRS) approach was proposed and properly optimized in [21] so that the sum-rate can be maximized. Apart from the difficulties in acquiring perfect CSIT, another consideration is the frame-based structure of multibeam satellite standards such as DVB-S2X [22]. Each spot beam of the satellite serves more than one user simultaneously by transmitting a single coded frame. Multiple users within the same beam share the same precoding vector. Such multibeam multicast transmission is a promising solution for the rapidly growing content-centric applications including video streaming, advertisements, large scale system updates and localized services, etc.

Motivated by the above practical issues in STIN, advanced multiple access techniques and interference management strategies are required. Rate-splitting multiple access (RSMA) has recently emerged as a promising non-orthogonal transmission for downlink multi-antenna wireless networks owning to its capability to enhance the system performance in a wide range of network loads, user deployments and CSIT qualities. RSMA was shown analytically in [23] to generalize four seemingly different strategies, namely space division multiple access (SDMA), power-domain non-orthogonal multiple access (NOMA), orthogonal multiple access (OMA) and physical-layer multicasting. The key behind the flexibility and robust manner of RSMA is to split each message into a common part and a private part. For the simplest implementation known as one-layer RSMA [24], [25], all the common parts are combined and jointly encoded as a single common stream to be decoded by all users, whereas the private messages are encoded individually as private streams. One-layer RSMA requires only one layer of SIC at each receiver. User grouping and ordering are not required since each user decodes the common stream before decoding its private stream. Compared with the generalized RSMA elaborated in [26], which involves multiple common streams and requires multiple SIC layers at the receivers, the encoding complexity, scheduling complexity and receiver complexity are reduced tremendously. Results in [26] show that the low complexity one-layer RSMA has a comparable rate performance to the generalized RSMA. The advantage of complexity reduction becomes more significant when the user number increases. By adjusting how much is carried by the common stream and how much is carried by the private streams, we adjust how much interference is decoded and how much interference is treated as noise. The benefits achieved by RSMA have been demonstrated in various multi-antenna terrestrial scenarios, such as multiuser unicast systems with perfect CSIT [23], [26]–[28] and imperfect CSIT [24], [29]–[32], and multigroup multicast systems [25], [33], [34]. The superior performance of RSMA can also be seen in massive MIMO systems with residual transceiver hardware impairments [35], mmWave communications [36], simultaneous wireless information and power transfer (SWIPT) networks [37] and radar-communication (RadCom) systems [38].

More recently, the use of RSMA in multibeam SatCom or integrated satellite systems has been investigated. Caus *et al.* [39] studied RSMA in a two-beam satellite system adopting time division multiplexing (TDM) in each beam. Vazquez *et al.* [40] focused on the sum-rate optimization and low complexity RSMA precoding design by decoupling the design of common stream and private streams. Yin and Clerckx [41], [42] proposed a RSMA-based multibeam multicast beamforming scheme and formulated a max-min fair (MMF) problem with different CSIT qualities. In [43], RSMA was proven to be promising for multigateway multibeam satellite systems with feeder link interference. Lin *et al.* [44] considered a satellite and aerial integrated network comprising a satellite and a unmanned aerial vehicle (UAV). The satellite employed multicast transmission, while the UAV used RSMA to improve spectral efficiency. In [45], a secure beamforming scheme for STIN was presented, where the satellite served one earth station (ES) with K eavesdroppers (Eves). RSMA was employed at the BS to achieve higher spectral efficiency. A robust beamforming scheme was proposed to maximize the secrecy energy efficiency of the ES considering Euclidean norm bounded channel uncertainty.

B. Contributions

Motivated by the prior works, we further investigate the application of RSMA into STIN to manage the interference within and between both sub-networks. Practical challenges are considered, such as the per-feed constraints,

CSIT uncertainty, and multibeam multicast transmission due to the existing satellite communication standards [22]. The contributions of this article are summarized as follows.

- First, we present a multiuser downlink framework for the integrated network where the satellite exploits multibeam multicast communication to serve satellite users (SUs), while the terrestrial BS employs uniform planar array (UPA) and serves cellular users (CUs) in a densely populated area. We take into account multibeam satellite characteristics, including the array pattern, path loss and rain attenuation, thus building a more realistic channel model to evaluate the system performance. The GW operates as a control center to implement centralized processing and control the whole network. Based on such framework, the joint beamforming design arises so that the satellite and terrestrial sub-system can share the same radio spectrum resources and cooperate with each other. RSMA is used at both the satellite and the BS to mitigate the interference including inter-beam interference, intra-cell interference and interference between the two sub-systems. We investigate two scenarios of RSMA-based STIN, namely the *coordinated scheme*, and the *cooperative scheme*. For the *coordinated scheme*, the satellite and BS exchange CSI of both direct and interfering links at the GW, and coordinate beamforming to manage the interference. For the *cooperative scheme*, the satellite and BS exchange both CSI and data at the GW. All propagation links (including interfering ones) are exploited to carry useful data upon appropriate beamforming. This differs from the prior RSMA-based STIN paper [45], where RSMA was utilized only at the terrestrial sub-system, and the benefits of coordination and cooperation were not investigated.
- Second, for both *coordinated scheme* and *cooperative scheme*, we respectively formulate optimization problems to maximize the minimum fairness rate of the RSMA-based STIN amongst all users subject to the constraint of per-feed transmit power at the satellite and the constraint of sum transmit power at the BS. Such problems upgrade the application of RSMA to multibeam satellite communications and terrestrial networks to a more general case, therefore leading to a joint beamforming design so that the two sub-systems can cooperate with each other. This is the first work on the joint beamforming design of RSMA-based *coordinated* STIN and *cooperative* STIN. Since the original optimization problem is non-convex, we apply the sequential convex approximation (SCA) to reformulate the original problem into an approximately equivalent convex one, which belongs to a second order cone problem (SOCP) and can be solved iteratively. The *cooperative scheme* is shown to outperform the *coordinated scheme* due to data exchange between the satellite and BS at the GW. Multiple baseline strategies are considered, including SDMA, NOMA, a two-step beamforming and fractional frequency reuse. Simulation results demonstrate the superiority of the proposed RSMA-based *cooperative scheme* and *coordinated scheme* compared with the baseline strategies.

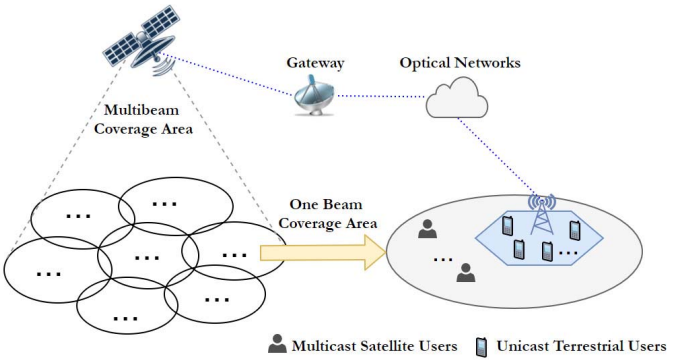

Fig. 1. Model of a satellite-terrestrial integrated network.

- Third, since it is in general very challenging to acquire accurate satellite CSI at the GW due to the round-trip delay and device mobility, we develop an expectation-based robust beamforming design against satellite channel phase uncertainty. For both RSMA-based *coordinated* STIN and *cooperative* STIN, non-convex MMF problems are formulated. To tackle the nonconvexity of the robust design, a novel iterative algorithm is proposed using SCA combining with a penalty function. Simulation results verify the effectiveness and robustness of the proposed RSMA schemes for STIN.

The rest of this paper is organized as follows. The system model, channel models and two schemes of RSMA-based STIN are introduced in Section II. Section III investigates the design of a joint beamforming scheme to achieve max-min fairness with the assumption of perfect CSIT. Section IV concentrates on a robust jont beamforming scheme in the presence of satellite channel phase uncertainty. Simulation results are given in Section V to evaluate the effectiveness of the proposed algorithms. Finally, we conclude this paper in Section VI.

Notations: In the remainder of this paper, boldface uppercase, boldface lowercase and standard letters denote matrices, column vectors, and scalars respectively. $\mathbb{R}$ and $\mathbb{C}$ denote the real and complex domains. $\mathbb{E}\left(\cdot\right)$ is the expectation of a random variable. The operators $\left(\cdot\right)^T$ and $\left(\cdot\right)^H$ denote the transpose and the Hermitian transpose. $|\cdot|$ and $\|\cdot\|$ denote the absolute value and Euclidean norm respectively. The real part of a complex number x is represented by $\mathcal{R}\left(x\right)$.

II. System Model

As illustrated in Fig. 1, we consider a STIN system employing full frequency reuse, where all SUs and CUs operate in the same frequency band. A geostationary orbit (GEO) satellite is equipped with an array fed reflector antenna. It provides services to the SUs that lack terrestrial access in sparsely populated or remote areas. By assuming a single feed per beam (SFPB) architecture, the array fed reflector antenna comprises a feed array with N_s feeds and generates N_s adjacent beams. Within the multibeam coverage area, we assume K_s SUs, and $\rho = \frac{K_s}{N_s}$ users in each beam. Since the SUs of one beam are served simultaneously by transmitting a single coded frame following DVB-S2X, the GEO satellite implements

multibeam multicast transmission. Meanwhile, the terrestrial BS[1] equipped with N_t-antenna uniform planar array (UPA) serves densely populated areas in the same frequency band. $K_t \leq N_t$ unicast CUs are assumed. User mobility is not considered in this work. Spectrum sharing is able to improve spectrum efficiency, which also leads to interference in and between the terrestrial and satellite sub-networks. As shown in Fig. 1, the GW acts as a control center to collect and manage various kinds of information, implement centralized processing and control the whole STIN. Optimal resource allocation and interference management on the satellite and BS can be jointly implemented at the GW to improve system performance.

A. Satellite Channel Model

Considering the free space loss, radiation pattern and rain attenuation of satellite channels, the downlink channel from the satellite to SU-k_s can be expressed as [42], [46]

$$\mathbf{f}_{k_s} = \mathbf{b}_{k_s} \circ \mathbf{q}_{k_s} \circ \exp\left\{j\boldsymbol{\phi}_{k_s}\right\}, \tag{1}$$

where $\circ$ is the Hadamard product. $\mathbf{b}_{k_s}$ is composed of free space loss and satellite beam radiation pattern. The n_s-th element of $\mathbf{b}_{k_s}$ is modeled as

$$b_{k_s,n_s} = \frac{\sqrt{G_R G_{k_s,n_s}}}{4\pi\frac{d_{k_s}}{\lambda}\sqrt{\kappa T_{sys} B_w}}, \tag{2}$$

where G_R is the user terminal antenna gain, d_{k_s} is the distance between SU-k_s and the satellite, λ is the carrier wavelength, κ is the Boltzmann constant, T_{sys} is the receiving system noise temperature and B_w denotes the bandwidth. The beam gain from the feed-n_s to SU-k_s can be approximated by

$$G_{k_s,n_s} = G_{max}\Big[\frac{J_1\left(u_{k_s,n_s}\right)}{2u_{k_s,n_s}} + 36\frac{J_3\left(u_{k_s,n_s}\right)}{u^3_{k_s,n_s}}\Big]^2, \tag{3}$$

where $u_{k_s,n_s} = 2.07123\sin\left(\theta_{k_s,n_s}\right)/\sin\left(\theta_{3\text{dB}}\right)$. Given the k_s-th SU position, θ_{k_s,n_s} is the angle between it and the center of beam-n_s with respect to the satellite, and $\theta_{3\text{dB}}$ is the 3 dB loss angle compared with the beam center. The maximum beam gain observed at each beam center is denoted by G_{max}. J_1 and J_3 are respectively the first-kind Bessel functions with order 1 and 3. The rain attenuation effect is characterized in $\mathbf{q}_{k_s} = \left[q_{k_s,1}, q_{k_s,2}, \cdots, q_{k_s,N_S}\right]^T$ with elements $q_{k_s,n_s} = \chi^{1/2}_{k_s,n_s}$. The dB form $\chi^{dB}_{k_s,n_s} = 20\log_{10}\left(\chi_{k_s,n_s}\right)$ is commonly modeled as a log-normal random variable, i.e., $\ln(\chi^{dB}_{k_s,n_s}) \sim \mathcal{N}\left(\mu,\sigma\right)$. Moreover, $\boldsymbol{\phi}_{k_s} = \left[\phi_{k_s,1}, \phi_{k_s,2}, \cdots, \phi_{k_s,N_S}\right]^T$ is a N_s-dimensional phase vector with each element uniformly distributed between 0 and 2π. The satellite channel matrix between the satellite and all SUs is denoted by $\mathbf{F} = [\mathbf{f}_1, \cdots, \mathbf{f}_{K_s}] \in \mathbb{C}^{N_s \times K_s}$. Similarly, when we consider $n_s \in \{1, \cdots, N_s\}$ and $k_t \in \{1, \cdots, K_t\}$, the interfering channel matrix between the satellite and all CUs is formulated by $\mathbf{Z} = [\mathbf{z}_1, \cdots, \mathbf{z}_{K_t}] \in \mathbb{C}^{N_s \times K_t}$.

[1]In this work, a unique BS is considered. The setting of multiple BSs is not considered here and is left for future studies.

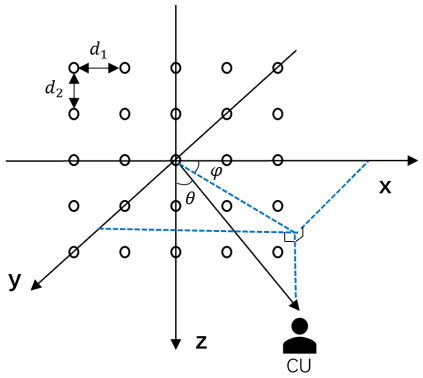

Fig. 2. Geometry of uniform planar array employed at the BS.

B. Terrestrial Channel Model

As illustrated in Fig. 2, we assume UPA at the BS with dimension $N_t = N_1 \times N_2$. N_1 and N_2 are respectively the number of array elements uniformly employed along the X-axis and the Z-axis. Due to the characteristic of radio wave propagation at high frequency band, the terrestrial channels can be expressed by a model consisting of L scatters. Each scatter contributes to a single propagation path. Mathematically, the downlink channel between the BS and CU k_t is given by [47]

$$\mathbf{h}_{k_t} = \sqrt{\frac{1}{L}}\sum_{l=1}^{L}\alpha_{k_t,l}\mathbf{a}_h\left(\theta_{k_t,l},\varphi_{k_t,l}\right) \otimes \mathbf{a}_v\left(\theta_{k_t,l}\right), \tag{4}$$

where $\alpha_{k_t,l}$ is the complex channel gain of the l-th path. Each $\alpha_{k_t,l}$ is assumed to follow independent and identical distribution (i.i.d.) $\mathcal{CN}\left(0,1\right)$. By denoting $\theta_{k_t,l}$ and $\varphi_{k_t,l}$ as the vertical and horizontal angles of the l-th path, and $\mathbf{r}_{n_1,n_2} = \left[x_{n_1}, 0, z_{n_2}\right]^T$ as the location of the (n_1,n_2)-th element, the horizontal steering vector $\mathbf{a}_h\left(\theta_{k_t,l},\varphi_{k_t,l}\right)$ and the vertical steering vector $\mathbf{a}_v(\theta_{k_t,l})$ are respectively

$$\begin{aligned}\mathbf{a}_h\left(\theta_{k_t,l},\varphi_{k_t,l}\right) = \big[&e^{-j\frac{2\pi}{\lambda}(\frac{N_1-1}{2})d_1\sin\theta_{k_t,l}\cos\varphi_{k_t,l}}, \cdots, \\ &e^{+j\frac{2\pi}{\lambda}(\frac{N_1-1}{2})d_1\sin\theta_{k_t,l}\cos\varphi_{k_t,l}}\big]^T,\end{aligned} \tag{5}$$

$$\begin{aligned}\mathbf{a}_v\left(\theta_{k_t,l}\right) = \big[&e^{-j\frac{2\pi}{\lambda}(\frac{N_2-1}{2})d_2\cos\theta_{k_t,l}}, \cdots, \\ &e^{+j\frac{2\pi}{\lambda}(\frac{N_2-1}{2})d_2\cos\theta_{k_t,l}}\big]^T,\end{aligned} \tag{6}$$

The terrestrial channel matrix between the BS and all CUs is denoted by $\mathbf{H} = [\mathbf{h}_1, \cdots, \mathbf{h}_{K_t}] \in \mathbb{C}^{N_t \times K_t}$.

C. Coordinated Scheme and Cooperative Scheme

In this work, we consider two levels of integration between the satellite and terrestrial BS.

1) Coordinated Scheme: First, we consider the basic level of integration where the CSI of both direct and interfering links of the whole network is available at the GW, while data is not exchanged between the satellite and BS at the GW. We call such scheme a *coordinated scheme*. It allows the satellite and BS to coordinate power allocation and beamforming directions to suppress interference. Different multiple access strategies can be exploited at the satellite and BS, such as RSMA,

SDMA, NOMA, etc. Here, we elaborate on the scenario where RSMA[2] is used at both the BS and satellite. To that end, the unicast messages $W_1, \cdots, W_{K_t}$ intended to CUs indexed by $\mathcal{K}_t = \{1, \cdots, K_t\}$ are split into common parts and private parts, i.e., $W_{k_t} \rightarrow \{W_{c,k_t}, W_{p,k_t}\}, \forall k_t \in \mathcal{K}_t$. All common parts are combined into W_c and encoded into a common stream s_c to be decoded by all CUs. All private parts are independently encoded into private streams $s_1, \cdots, s_{K_t}$. The vector of BS streams $\mathbf{s} = [s_c, s_1, \cdots, s_{K_t}]^T \in \mathbb{C}^{(K_t+1)\times 1}$ is therefore created, and we suppose it obeying $\mathbb{E}\{\mathbf{s}\mathbf{s}^H\} = \mathbf{I}$. For the satellite, multicast messages $M_1, \cdots M_{N_s}$ are intended to the beams indexed by $\mathcal{N}_s = \{1, \cdots, N_s\}$. Each message $M_{n_s}, \forall n_s \in \mathcal{N}_s$ is split into a common part M_{c,n_s} and a private part M_{p,n_s}. All common parts are combined as M_c and encoded into m_c, while all private parts are independently encoded into $m_1, \cdots, m_{N_s}$. The vector of satellite streams $\mathbf{m} = [m_c, m_1, \cdots, m_{N_s}]^T \in \mathbb{C}^{(N_s+1)\times 1}$ is obtained, and we assume it satisfying $\mathbb{E}\{\mathbf{m}\mathbf{m}^H\} = \mathbf{I}$. Both $\mathbf{s}$ and $\mathbf{m}$ are linearly precoded. The transmitted signals at the satellite and BS are respectively

$$\mathbf{x}^{sat} = \mathbf{w}_c m_c + \sum_{n_s=1}^{N_s} \mathbf{w}_{n_s} m_{n_s}, \tag{7}$$

$$\mathbf{x}^{bs} = \mathbf{p}_c s_c + \sum_{k_t=1}^{K_t} \mathbf{p}_{k_t} s_{k_t}, \tag{8}$$

where $\mathbf{W} = [\mathbf{w}_c, \mathbf{w}_1, \cdots, \mathbf{w}_{N_s}] \in \mathbb{C}^{N_s\times(N_s+1)}$ and $\mathbf{P} = [\mathbf{p}_c, \mathbf{p}_1, \cdots, \mathbf{p}_{K_t}] \in \mathbb{C}^{N_t\times(K_t+1)}$ are defined as the beamforming matrices at the satellite and BS. m_c and s_c are superimposed on top of the private signals. Even though power sharing mechanisms among beams can be implemented by using, e.g., multi-port amplifiers [48], the deployment of satellite payloads allowing flexible power allocation will require costly and complex radio-frequency designs. Thus, a per-feed transmit power constraint is considered, which is given by $(\mathbf{W}\mathbf{W}^H)_{n_s,n_s} \leq \frac{P_s}{N_s}$, $\forall n_s \in \mathcal{N}_s$. The sum transmit power constraint of BS is given by $\mathrm{tr}(\mathbf{P}\mathbf{P}^H) \leq P_t$. Based on the channel models defined above, the received signal at each SU-k_s writes as

$$y_{k_s}^{sat} = \mathbf{f}_{k_s}^H \mathbf{w}_c m_c + \mathbf{f}_{k_s}^H \sum_{i=1}^{N_s} \mathbf{w}_i m_i + n_{k_s}^{sat}. \tag{9}$$

Since we assume all SUs are located outside the BS service area, each SU sees multibeam interference and no interference from the BS. The received signal at each CU-k_t writes as

$$y_{k_t}^{bs} = \mathbf{h}_{k_t}^H \mathbf{p}_c s_c + \mathbf{h}_{k_t}^H \sum_{j=1}^{K_t} \mathbf{p}_j s_j + \mathbf{z}_{k_t}^H \mathbf{w}_c m_c + \mathbf{z}_{k_t}^H \sum_{i=1}^{N_s} \mathbf{w}_i m_i + n_{k_t}^{bs}. \tag{10}$$

Each CU suffers from intra-cell interference and from satellite interference. $\mathbf{z}_1, \cdots, \mathbf{z}_{Kt}$ represent satellite interfering channels. $n_{k_s}^{sat}$ and $n_{k_t}^{bs}$ are the additive Gaussian white noises (AWGN) with zero mean and variance $\sigma_{k_s}^{sat2}$ and $\sigma_{k_t}^{bs2}$ respectively. For both SUs and CUs, the common stream is firstly decoded while treating the other interference as noise. The SINRs of decoding the common stream at SU-k_s and CU-k_t are given by

$$\gamma_{c,k_s}^{sat} = \frac{\left|\mathbf{f}_{k_s}^H \mathbf{w}_c\right|^2}{\sum_{i=1}^{N_s} \left|\mathbf{f}_{k_s}^H \mathbf{w}_i\right|^2 + \sigma_{k_s}^{sat2}}, \tag{11}$$

$$\gamma_{c,k_t}^{bs} = \frac{\left|\mathbf{h}_{k_t}^H \mathbf{p}_c\right|^2}{\sum_{j=1}^{K_t} \left|\mathbf{h}_{k_t}^H \mathbf{p}_j\right|^2 + \left|\mathbf{z}_{k_t}^H \mathbf{w}_c\right|^2 + \sum_{i=1}^{N_s} \left|\mathbf{z}_{k_t}^H \mathbf{w}_i\right|^2 + \sigma_{k_t}^{bs2}}. \tag{12}$$

Given perfect CSIT, the achievable rate of the common streams are $R_{c,k_s}^{sat} = \log_2(1 + \gamma_{c,k_s}^{sat})$ and $R_{c,k_t}^{bs} = \log_2(1 + \gamma_{c,k_t}^{bs})$. To guarantee that each SU is capable of decoding m_c, and each CU is capable of decoding s_c, they must be transmitted at rates that do not exceed

$$R_c^{sat} = \min_{k_s \in \mathcal{K}_s} \{R_{c,k_s}^{sat}\} = \sum_{n_s=1}^{N_s} C_{n_s}^{sat}, \tag{13}$$

$$R_c^{bs} = \min_{k_t \in \mathcal{K}_t} \{R_{c,k_t}^{bs}\} = \sum_{k_t=1}^{K_t} C_{k_t}^{bs}, \tag{14}$$

where $C_{n_s}^{sat}$ is the portion of the common part of the n_s-th beam's message. $C_{k_t}^{bs}$ is the portion of the common part of the k_t-th CU's message. After the common stream is re-encoded, precoded and subtracted from the received signal through SIC, each user then decodes its desired private stream. We define $\mu : \mathcal{K}_s \rightarrow \mathcal{N}_s$ as mapping a SU to its corresponding beam. The SINRs of decoding $m_{\mu(k_s)}$ at SU-k_s and decoding s_{k_t} at CU-k_t are given by

$$\gamma_{k_s}^{sat} = \frac{\left|\mathbf{f}_{k_s}^H \mathbf{w}_{\mu(k_s)}\right|^2}{\sum_{i=1, i\neq\mu(k_s)}^{N_s} \left|\mathbf{f}_{k_s}^H \mathbf{w}_i\right|^2 + \sigma_{k_s}^{sat2}}, \tag{15}$$

$$\gamma_{k_t}^{bs} = \frac{\left|\mathbf{h}_{k_t}^H \mathbf{p}_{k_t}\right|^2}{\sum_{j=1, j\neq k_t}^{K_t} \left|\mathbf{h}_{k_t}^H \mathbf{p}_j\right|^2 + \left|\mathbf{z}_{k_t}^H \mathbf{w}_c\right|^2 + \sum_{i=1}^{N_s} \left|\mathbf{z}_{k_t}^H \mathbf{w}_i\right|^2 + \sigma_{k_t}^{bs2}}. \tag{16}$$

The achievable rates of the private streams are respectively $R_{k_s}^{sat} = \log_2(1 + \gamma_{k_s}^{sat})$ and $R_{k_t}^{bs} = \log_2(1 + \gamma_{k_t}^{bs})$. Thus, the achievable rates of the n_s-th beam and k_t-th CU respectively write as

$$R_{\mathrm{tot},n_s}^{sat} = C_{n_s}^{sat} + \min_{i \in \mathcal{G}_{n_s}} R_i^{sat} \quad \text{and} \quad R_{\mathrm{tot},k_t}^{bs} = C_{k_t}^{bs} + R_{k_t}^{bs}, \tag{17}$$

where $\mathcal{G}_{n_s}$ denotes the set of SUs belonging to the n_s-th beam.

2) Cooperative Scheme: Second, we consider a higher level of integration, i.e., *cooperative scheme* where both CSI and data are exchanged between the satellite and BS at the GW. In this scenario, all downlink messages $W_1, \cdots, W_{K_t}$ intended to CUs, and multicast messages $M_1, \cdots, M_{N_s}$ intended to SUs are transmitted at both the satellite and BS.

[2]RSMA has been shown analytically as a general multiple access strategy, which boils down to SDMA and NOMA when allocating powers to the different types of message streams [23].

All propagation links (including interfering ones) are exploited to carry useful data upon appropriate beamforming. We still consider RSMA to manage interference in this *cooperative STIN*, including inter-beam interference, intra-cell interference and interference between the satellite and terrestrial sub-networks. Each message is split into a common part and a private part. All common parts are encoded together into a super common stream shared by all users in the system. As a result, the symbol stream to be transmitted is given by $\acute{\mathbf{s}} = [\acute{s}_c, \acute{m}_1, \cdots, \acute{m}_{N_s}, \acute{s}_1, \cdots, \acute{s}_{K_t}]^T \in \mathcal{C}^{N_s+K_t+1}$. Throughout this work, we use "$\acute{}$" to differentiate notations in the *cooperative scheme* and the above *coordinated scheme*. The transmitted signals at the satellite writes as

$$\acute{\mathbf{x}}^{sat} = \acute{\mathbf{w}}_c \acute{s}_c + \sum_{i=1}^{N_s} \acute{\mathbf{w}}_i^{sat} \acute{m}_i + \sum_{j=1}^{K_t} \acute{\mathbf{w}}_j^{bs} \acute{s}_j, \tag{18}$$

where $\acute{\mathbf{W}} = \left[\acute{\mathbf{w}}_c, \acute{\mathbf{w}}_1^{sat}, \cdots, \acute{\mathbf{w}}_{N_s}^{sat}, \acute{\mathbf{w}}_1^{bs}, \cdots, \acute{\mathbf{w}}_{K_t}^{bs}\right]$ is the beamforming matrix, and the superscripts of $\acute{\mathbf{w}}_i^{sat}$ and $\acute{\mathbf{w}}_j^{bs}$ are used to differentiate the precoder of satellite data and BS data. The per-feed transmit power constraint writes as $(\acute{\mathbf{W}}\acute{\mathbf{W}}^H)_{n_s,n_s} \leq \frac{P_s}{N_s}$, $\forall n_s \in \mathcal{N}_s$. Similarly, the transmitted signal at the BS writes as

$$\acute{\mathbf{x}}^{bs} = \acute{\mathbf{p}}_c \acute{s}_c + \sum_{i=1}^{N_s} \acute{\mathbf{p}}_i^{sat} \acute{m}_i + \sum_{j=1}^{K_t} \acute{\mathbf{p}}_j^{bs} \acute{s}_j, \tag{19}$$

where $\acute{\mathbf{P}} = \left[\acute{\mathbf{p}}_c, \acute{\mathbf{p}}_1^{sat}, \cdots, \acute{\mathbf{p}}_{N_s}^{sat}, \acute{\mathbf{p}}_1^{bs}, \cdots, \acute{\mathbf{p}}_{K_t}^{bs}\right]$ is the beamforming matrix, and the sum transmit power constraint of the BS is $\mathrm{tr}(\acute{\mathbf{P}}\acute{\mathbf{P}}^H) \leq P_t$. Accordingly, the received signal at SU-k_s is given by

$$\acute{y}_{k_s}^{sat} = \mathbf{f}_{k_s}^H \acute{\mathbf{w}}_c \acute{s}_c + \mathbf{f}_{k_s}^H \sum_{i=1}^{N_s} \acute{\mathbf{w}}_i^{sat} \acute{m}_i + \mathbf{f}_{k_s}^H \sum_{j=1}^{K_t} \acute{\mathbf{w}}_j^{bs} \acute{s}_j + \acute{n}_{k_s}^{sat}. \tag{20}$$

The received signal at CU-k_t is given by

$$\begin{aligned}\acute{y}_{k_t}^{bs} = {} & \mathbf{h}_{k_t}^H \acute{\mathbf{p}}_c \acute{s}_c + \mathbf{h}_{k_t}^H \sum_{j=1}^{K_t} \acute{\mathbf{p}}_j^{bs} \acute{s}_j + \mathbf{h}_{k_t}^H \sum_{i=1}^{N_s} \acute{\mathbf{p}}_i^{sat} \acute{m}_i \\ & + \mathbf{z}_{k_t}^H \acute{\mathbf{w}}_c \acute{s}_c + \mathbf{z}_{k_t}^H \sum_{i=1}^{N_s} \acute{\mathbf{w}}_i^{sat} \acute{m}_i + \mathbf{z}_{k_t}^H \sum_{j=1}^{K_t} \acute{\mathbf{w}}_j^{bs} \acute{s}_j + \acute{n}_{k_t}^{bs}.\end{aligned} \tag{21}$$

To simplify (21), aggregate channels and aggregate beamforming vectors are defined by

$$\mathbf{g}_{k_t} = \left[\mathbf{z}_{k_t}^H, \mathbf{h}_{k_t}^H\right]^H \in \mathbb{C}^{(N_s+N_t)\times 1}, \quad \forall k_t \in \mathcal{K}_t, \tag{22}$$

$$\mathbf{v}_c = \left[\mathbf{w}_c^{*H}, \mathbf{p}_c^{*H}\right]^H \in \mathbb{C}^{(N_s+N_t)\times 1}, \tag{23}$$

$$\mathbf{v}_{n_s}^{sat} = \left[\acute{\mathbf{w}}_{n_s}^{satH}, \acute{\mathbf{p}}_{n_s}^{satH}\right]^H \in \mathbb{C}^{(N_s+N_t)\times 1}, \quad \forall n_s \in \mathcal{N}_s, \tag{24}$$

$$\mathbf{v}_{k_t}^{bs} = \left[\acute{\mathbf{w}}_{k_t}^{bsH}, \acute{\mathbf{p}}_{k_t}^{bsH}\right]^H \in \mathbb{C}^{(N_s+N_t)\times 1}, \quad \forall k_t \in \mathcal{K}_t. \tag{25}$$

The received signal at CU-k_t can be rewritten as

$$\acute{y}_{k_t}^{bs} = \mathbf{g}_{k_t}^H \mathbf{v}_c \acute{s}_c + \mathbf{g}_{k_t}^H \sum_{j=1}^{K_t} \mathbf{v}_j^{bs} \acute{s}_j + \mathbf{g}_{k_t}^H \sum_{i=1}^{N_s} \mathbf{v}_i^{sat} \acute{m}_i + \acute{n}_{kt}^{bs}. \tag{26}$$

Satellite interfering links are exploited to carry terrestrial data so as to improve the performance of STIN. The aggregate beamforming vectors are collected into a matrix

$$\begin{aligned}\mathbf{V} = {} & [\mathbf{v}_c, \mathbf{v}_1^{sat}, \cdots, \mathbf{v}_{N_s}^{sat}, \mathbf{v}_1^{bs}, \cdots, \mathbf{v}_{K_t}^{bs}] \\ & \in \mathbb{C}^{(N_s+N_t)\times(N_s+K_t+1)},\end{aligned} \tag{27}$$

which can also be denoted by $\mathbf{V} = [\acute{\mathbf{W}}^H, \acute{\mathbf{P}}^H]^H$. For both SUs and CUs, the common stream is firstly decoded and removed from the received signal through SIC. The SINRs of decoding $\acute{s}_c$ at the k_s-th SU and the k_t-th CU are respectively

$$\acute{\gamma}_{c,k_s}^{sat} = \frac{\left|\mathbf{f}_{k_s}^H \acute{\mathbf{w}}_c\right|^2}{\sum_{i=1}^{N_s} \left|\mathbf{f}_{k_s}^H \acute{\mathbf{w}}_i^{sat}\right|^2 + \sum_{j=1}^{K_t} \left|\mathbf{f}_{k_s}^H \acute{\mathbf{w}}_j^{bs}\right|^2 + \sigma_{k_s}^{sat2}}, \tag{28}$$

$$\acute{\gamma}_{c,k_t}^{bs} = \frac{\left|\mathbf{g}_{k_t}^H \mathbf{v}_c\right|^2}{\sum_{j=1}^{K_t} \left|\mathbf{g}_{k_t}^H \mathbf{v}_j^{bs}\right|^2 + \sum_{i=1}^{N_s} \left|\mathbf{g}_{k_t}^H \mathbf{v}_i^{sat}\right|^2 + \sigma_{k_t}^{bs2}}. \tag{29}$$

The corresponding achievable rates are $\acute{R}_{c,k_s}^{sat} = \log_2(1+\acute{\gamma}_{c,k_s}^{sat})$ and $\acute{R}_{c,k_t}^{bs} = \log_2(1+\acute{\gamma}_{c,k_t}^{bs})$. Since $\acute{s}_c$ is decoded by all users in the system, we define the common rate as

$$\acute{R}_c = \min_{k_s\in\mathcal{K}_s, k_t\in\mathcal{K}_t} \left\{\acute{R}_{c,k_s}^{sat}, \acute{R}_{c,k_t}^{bs}\right\} = \sum_{n_s=1}^{N_s} \acute{C}_{n_s}^{sat} + \sum_{k_t=1}^{K_t} \acute{C}_{k_t}^{bs}. \tag{30}$$

Note that $\acute{s}_c$ is shared amongst all satellite beams and CUs. $\acute{C}_{n_s}^{sat}$ and $\acute{C}_{k_t}^{bs}$ respectively correspond to the beam-n_s's and CU-k_t's portion of common rate. After removing $\acute{s}_c$ using SIC, each user then decodes its desired private stream. The SINRs of decoding private streams are

$$\acute{\gamma}_{k_s}^{sat} = \frac{\left|\mathbf{f}_{k_s}^H \acute{\mathbf{w}}_{\mu(k_s)}^{sat}\right|^2}{\sum_{i=1, i\neq\mu(k_s)}^{N_s} \left|\mathbf{f}_{k_s}^H \acute{\mathbf{w}}_i^{sat}\right|^2 + \sum_{j=1}^{K_t} \left|\mathbf{f}_{k_s}^H \acute{\mathbf{w}}_j^{bs}\right|^2 + \sigma_{k_s}^{sat2}}, \tag{31}$$

$$\acute{\gamma}_{k_t}^{bs} = \frac{\left|\mathbf{g}_{k_t}^H \mathbf{v}_{k_t}^{bs}\right|^2}{\sum_{j=1, j\neq k_t}^{K_t} \left|\mathbf{g}_{k_t}^H \mathbf{v}_j^{bs}\right|^2 + \sum_{i=1}^{N_s} \left|\mathbf{g}_{k_t}^H \mathbf{v}_i^{sat}\right|^2 + \sigma_{k_t}^{bs2}}. \tag{32}$$

$\acute{R}_{k_s}^{sat} = \log_2(1+\acute{\gamma}_{k_s}^{sat})$ and $\acute{R}_{k_t}^{bs} = \log_2(1+\acute{\gamma}_{k_t}^{bs})$ are the achievable rates of the private streams. Thus, the achievable rates of the n_s-th beam and k_t-th CU respectively write as

$$\acute{R}_{\mathrm{tot},n_s}^{sat} = \acute{C}_{n_s}^{sat} + \min_{i\in\mathcal{G}_{n_s}} \acute{R}_i^{sat} \quad \text{and} \quad \acute{R}_{\mathrm{tot},k_t}^{bs} = \acute{C}_{k_t}^{bs} + \acute{R}_{k_t}^{bs}. \tag{33}$$

From the above expressions, we can regard the satellite and BS working together as a super "BS" but subject to their respective power constraints to serve the CUs and SUs. The super common stream contains parts of the unicast messages intended to the CUs, and parts of the multicast messages intended to the SUs. At each user side, the super common stream is firstly decoded and then removed through SIC. Accordingly, the interference is partially decoded. Each user then decodes its private stream and treats the remaining interference as noise. Such scheme has the capability to better manage interference including not only inter-beam interference, intra-cell interference, but also interference between the satellite and terrestrial sub-networks.

Remark 1: With the assumption of Gaussian signaling and infinite block length, there is no decoding error in SIC. Decoding error in SIC would only occur if we depart from Shannon assumptions and assume finite constellations and finite block lengths. We consider one-layer RSMA for either coordinated scheme and cooperative scheme. Only one layer of SIC is required at each terminals. The receiver complexity does not depend on the number of served users. The generalized RSMA and hierarchical RSMA described in [26] is able to provide more room for achievable rate enhancements at the expense of more layers of SIC at receivers. However, its implementation can be complex due to the large number of SIC layers and common messages involved. The receiver complexity of generalized RSMA and hierarchical RSMA increases with the number of served users. Moreover, ordering and grouping are not required in this one-layer RSMA architecture since all users decode the common stream before decoding their private streams. Both scheduling complexity and receiver complexity are reduced tremendously. Readers are referred to [26] and [49] for more details on complexity issues.

III. Proposed Joint Beamforming Scheme

In this section, the problem of interest is to design a joint beamforming scheme to maximize the minimum fairness rate amongst all unicast CUs and multibeam multicast SUs subject to transmit power constraints. We respectively consider the scenarios of RSMA-based *coordinated STIN* and *cooperative STIN* when we assume perfect CSI at the GW.

A. Joint Beamforming Design for Coordinated STIN

For RSMA-based *coordinated STIN*, the optimization problem to maximize the minimum fairness rate can be formulated as

$$\mathcal{P}_1: \max_{\mathbf{W},\mathbf{P},\mathbf{c}^{sat},\mathbf{c}^{bs}} \min_{n_s\in\mathcal{N}_s,k_t\in\mathcal{K}_t} \left\{R^{bs}_{\text{tot},k_t}, R^{sat}_{\text{tot},n_s}\right\} \quad (34)$$

$$s.t.\ R^{bs}_{c,k_t} \geq \sum_{j=1}^{K_t} C^{bs}_j, \quad \forall k_t \in \mathcal{K}_t \quad (35)$$

$$C^{bs}_{k_t} \geq 0, \quad \forall k_t \in \mathcal{K}_t \quad (36)$$

$$\text{tr}(\mathbf{P}\mathbf{P}^H) \leq P_t \quad (37)$$

$$R^{sat}_{c,k_s} \geq \sum_{j=1}^{N_s} C^{sat}_j, \quad \forall k_s \in \mathcal{K}_s \quad (38)$$

$$C^{sat}_{n_s} \geq 0, \quad \forall n_s \in \mathcal{N}_s \quad (39)$$

$$(\mathbf{W}\mathbf{W}^H)_{n_s,n_s} \leq \frac{P_s}{N_s}, \quad \forall n_s \in \mathcal{N}_s \quad (40)$$

where $\mathbf{c}^{sat} = [C^{sat}_1, \cdots, C^{sat}_{N_s}]^T$, $\mathbf{c}^{bs} = [C^{bs}_1, \cdots, C^{bs}_{K_t}]^T$ are the vectors of common rate portions. (35) guarantees that the common stream s_c can be decoded by all CUs. (37) is the sum transmit power constraint of the BS. Similarly, (38) ensures the common stream m_c to be decoded by all SUs. (40) represents the per-feed transmit power constraint of the satellite. (36) and (39) guarantee the non-negativity of all common rate portions. Note that the formulated problem is non-convex, we exploit an SCA-based method to convexify the non-convex constraints and approximate the non-convex problem to a convex one. First, we introduce an equivalent reformulation of $\mathcal{P}_1$, which is

$$\mathcal{E}_1: \max_{\mathbf{W},\mathbf{P},\mathbf{c}^{sat},\mathbf{c}^{bs},q,\mathbf{r},\boldsymbol{\alpha}} q \quad (41)$$

$$s.t.\ C^{bs}_{k_t} + \alpha_{k_t} \geq q, \quad \forall k_t \in \mathcal{K}_t \quad (42)$$

$$R^{bs}_{k_t} \geq \alpha_{k_t}, \quad \forall k_t \in \mathcal{K}_t \quad (43)$$

$$C^{sat}_{n_s} + r_{k_s} \geq q, \quad \forall k_s \in \mathcal{G}_{n_s} \quad (44)$$

$$R^{sat}_{k_s} \geq r_{k_s}, \quad \forall k_s \in \mathcal{K}_s \quad (45)$$

$$(35) - (40)$$

where q, $\boldsymbol{\alpha} = [\alpha_1, \cdots, \alpha_{K_t}]^T$, $\mathbf{r} = [r_1, \cdots, r_{K_s}]^T$ are newly introduced auxiliary variables. To deal with the nonconvexity of (35), (38), (43), (45), we further introduce new auxiliary variables $\mathbf{a} = [a_1, \cdots, a_{K_t}]^T$, $\mathbf{a}_c = [a_{c,1}, \cdots, a_{c,K_t}]^T$, $\mathbf{b} = [b_1, \cdots, b_{K_s}]^T$ and $\mathbf{b}_c = [b_{c,1}, \cdots, b_{c,K_s}]^T$. The problem $\mathcal{E}_1$ can be rewritten as

$$\mathcal{S}_1: \max_{q,\mathbf{W},\mathbf{P},\mathbf{c}^{sat},\mathbf{c}^{bs},\mathbf{r},\boldsymbol{\alpha},\mathbf{a},\mathbf{a}_c,\mathbf{b},\mathbf{b}_c} q \quad (46)$$

$$s.t.\ \log(1+a_{k_t}) \geq \alpha_{k_t}\log 2, \quad \forall k_t \in \mathcal{K}_t \quad (47)$$

$$\gamma^{bs}_{k_t} \geq a_{k_t}, \quad \forall k_t \in \mathcal{K}_t \quad (48)$$

$$\log(1+b_{k_s}) \geq r_{k_s}\log 2, \quad \forall k_s \in \mathcal{K}_s \quad (49)$$

$$\gamma^{sat}_{k_s} \geq b_{k_s}, \quad \forall k_s \in \mathcal{K}_s \quad (50)$$

$$\log(1+a_{c,k_t}) \geq \sum_{j=1}^{K_t} C^{bs}_j \log 2, \quad \forall k_t \in \mathcal{K}_t \quad (51)$$

$$\gamma^{bs}_{c,k_t} \geq a_{c,k_t}, \quad \forall k_t \in \mathcal{K}_t \quad (52)$$

$$\log(1+b_{c,k_s}) \geq \sum_{j=1}^{N_s} C^{sat}_j \log 2, \quad \forall k_s \in \mathcal{K}_s \quad (53)$$

$$\gamma^{sat}_{c,k_s} \geq b_{c,k_s}, \quad \forall k_s \in \mathcal{K}_s \quad (54)$$

$$(36), (37), (39), (40), (42), (44)$$

where (47) - (54) are obtained by extracting the SINRs from the rate expressions $R^{bs}_{k_t}, R^{sat}_{k_s}, R^{bs}_{c,k_t}, R^{sat}_{c,k_s}$ in (35), (38), (43), (45) of Problem $\mathcal{E}_1$. Since the constraints of $\mathcal{S}_1$ hold with equality at optimality, the equivalence between $\mathcal{P}_1$ and $\mathcal{S}_1$ can be guaranteed. Now, the nonconvexity of $\mathcal{S}_1$ comes from (48), (50), (52) and (54) which contain SINR expressions. (48) can be expanded as

$$\sum_{j=1,j\neq k_t}^{K_t} \left|\mathbf{h}^H_{k_t}\mathbf{p}_j\right|^2 + \left|\mathbf{z}^H_{k_t}\mathbf{w}_c\right|^2 + \sum_{i=1}^{N_s}\left|\mathbf{z}^H_{k_t}\mathbf{w}_i\right|^2 + \sigma^{bs2}_{k_t} \leq \frac{\left|\mathbf{h}^H_{k_t}\mathbf{p}_{k_t}\right|^2}{a_{k_t}}, \quad (55)$$

where the right-hand side (RHS) quadratic-over-linear function is convex. We approximate $\frac{\left|\mathbf{h}^H_{k_t}\mathbf{p}_{k_t}\right|^2}{a_{k_t}}$ with its lower bound, which is obtained by the first-order Taylor series approxima-

tion around the point $\left(\mathbf{p}_{k_t}^{[n]}, a_{k_t}^{[n]}\right)$. Then, we have

$$\frac{\left|\mathbf{h}_{k_t}^H \mathbf{p}_{k_t}\right|^2}{a_{k_t}} \geq \frac{2\mathcal{R}\left(\mathbf{p}_{k_t}^{[n]H}\mathbf{h}_{k_t}\mathbf{h}_{k_t}^H\mathbf{p}_{k_t}\right)}{a_{k_t}^{[n]}} - \frac{\mathbf{p}_{k_t}^{[n]H}\mathbf{h}_{k_t}\mathbf{h}_{k_t}^H\mathbf{p}_{k_t}^{[n]}}{\left(a_{k_t}^{[n]}\right)^2}a_{k_t} \triangleq \widehat{f}_1\left(\mathbf{p}_{k_t}, a_{k_t}; \mathbf{p}_{k_t}^{[n]}, a_{k_t}^{[n]}\right) \tag{56}$$

where n represents the n-th SCA iteration. Replacing the linear approximation $\widehat{f}_1\left(\mathbf{p}_{k_t}, a_{k_t}; \mathbf{p}_{k_t}^{[n]}, a_{k_t}^{[n]}\right)$ with the RHS of (55) yields

$$\sum_{j=1, j\neq k_t}^{K_t}\left|\mathbf{h}_{k_t}^H\mathbf{p}_j\right|^2 + \left|\mathbf{z}_{k_t}^H\mathbf{w}_c\right|^2 + \sum_{i=1}^{N_s}\left|\mathbf{z}_{k_t}^H\mathbf{w}_i\right|^2 + \sigma_{k_t}^{bs2} - \widehat{f}_1\left(\mathbf{p}_{k_t}, a_{k_t}; \mathbf{p}_{k_t}^{[n]}, a_{k_t}^{[n]}\right) \leq 0. \tag{57}$$

Similarly, the constraint (50) can be expanded as

$$\sum_{i=1, i\neq\mu(k_s)}^{N_s}\left|\mathbf{f}_{k_s}^H\mathbf{w}_i\right|^2 + \sigma_{k_s}^{sat2} \leq \frac{\left|\mathbf{f}_{k_s}^H\mathbf{w}_{\mu(k_s)}\right|^2}{b_{k_s}}. \tag{58}$$

We approximate its RHS around the point $\left(\mathbf{w}_{\mu(k_s)}^{[n]}, b_{k_s}^{[n]}\right)$, and obtain

$$\frac{\left|\mathbf{f}_{k_s}^H\mathbf{w}_{\mu(k_s)}\right|^2}{b_{k_s}} \geq \frac{2\mathcal{R}\left(\mathbf{w}_{\mu(k_s)}^{[n]H}\mathbf{f}_{k_s}\mathbf{f}_{k_s}^H\mathbf{w}_{\mu(k_s)}\right)}{b_{k_s}^{[n]}} - \frac{\mathbf{w}_{\mu(k_s)}^{[n]H}\mathbf{f}_{k_s}\mathbf{f}_{k_s}^H\mathbf{w}_{\mu(k_s)}^{[n]}}{\left(b_{k_s}^{[n]}\right)^2}b_{k_s} \triangleq \widehat{f}_2\left(\mathbf{w}_{\mu(k_s)}, b_{k_s}; \mathbf{w}_{\mu(k_s)}^{[n]}, b_{k_s}^{[n]}\right). \tag{59}$$

Replacing $\widehat{f}_2\left(\mathbf{w}_{\mu(k_s)}, b_{k_s}; \mathbf{w}_{\mu(k_s)}^{[n]}, b_{k_s}^{[n]}\right)$ with the RHS of (58) yields

$$\sum_{i=1, i\neq\mu(k_s)}^{N_s}\left|\mathbf{f}_{k_s}^H\mathbf{w}_i\right|^2 + \sigma_{k_s}^{sat2} - \widehat{f}_2\left(\mathbf{w}_{\mu(k_s)}, b_{k_s}; \mathbf{w}_{\mu(k_s)}^{[n]}, b_{k_s}^{[n]}\right) \leq 0. \tag{60}$$

Following the same logic, (52) and (54) are respectively approximated by

$$\left|\mathbf{h}_{k_t}^H\mathbf{p}_{k_t}\right|^2 + \sum_{j=1, j\neq k_t}^{K_t}\left|\mathbf{h}_{k_t}^H\mathbf{p}_j\right|^2 + \left|\mathbf{z}_{k_t}^H\mathbf{w}_c\right|^2 + \sum_{i=1}^{N_s}\left|\mathbf{z}_{k_t}^H\mathbf{w}_i\right|^2 + \sigma_{k_t}^{bs2} - \widehat{f}_3\left(\mathbf{p}_c, a_{c,k_t}; \mathbf{p}_c^{[n]}, a_{c,k_t}^{[n]}\right) \leq 0, \tag{61}$$

$$\left|\mathbf{f}_{k_s}^H\mathbf{w}_{\mu(k_s)}\right|^2 + \sum_{i=1, i\neq\mu(k_s)}^{N_s}\left|\mathbf{f}_{k_s}^H\mathbf{w}_i\right|^2 + \sigma_{k_s}^{sat2} - \widehat{f}_4\left(\mathbf{w}_c, b_{c,k_s}; \mathbf{w}_c^{[n]}, b_{c,k_s}^{[n]}\right) \leq 0, \tag{62}$$

where $\widehat{f}_3\left(\mathbf{p}_c, a_{c,k_t}; \mathbf{p}_c^{[n]}, a_{c,k_t}^{[n]}\right)$ and $\widehat{f}_4\left(\mathbf{w}_c, b_{c,k_s}; \mathbf{w}_c^{[n]}, b_{c,k_s}^{[n]}\right)$ are linear lower bound expressions

$$\widehat{f}_3\left(\mathbf{p}_c, a_{c,k_t}; \mathbf{p}_c^{[n]}, a_{c,k_t}^{[n]}\right) \triangleq \frac{2\mathcal{R}\left(\mathbf{p}_c^{[n]H}\mathbf{h}_{k_t}\mathbf{h}_{k_t}^H\mathbf{p}_c\right)}{a_{c,k_t}^{[n]}} - \frac{\mathbf{p}_c^{[n]H}\mathbf{h}_{k_t}\mathbf{h}_{k_t}^H\mathbf{p}_c^{[n]}}{\left(a_{c,k_t}^{[n]}\right)^2}a_{c,k_t}, \tag{63}$$

$$\widehat{f}_4\left(\mathbf{w}_c, b_{c,k_s}; \mathbf{w}_c^{[n]}, b_{c,k_s}^{[n]}\right) \triangleq \frac{2\mathcal{R}\left(\mathbf{w}_c^{[n]H}\mathbf{f}_{k_s}\mathbf{f}_{k_s}^H\mathbf{w}_c\right)}{b_{c,k_s}^{[n]}} - \frac{\mathbf{w}_c^{[n]H}\mathbf{f}_{k_s}\mathbf{f}_{k_s}^H\mathbf{w}_c^{[n]}}{\left(b_{c,k_s}^{[n]}\right)^2}b_{c,k_s}. \tag{64}$$

Although (47), (49), (51) and (53) are convex constraints, which are solvable through the CVX toolbox in Matlab, the log terms belong to generalized nonlinear convex program with high computational complexity. Aiming at more efficient implementation, [50] approximates the log constraints to a set of second-order cone (SOC) constraints, which introduce a great number of slack variables and result in an increase of per-iteration complexity. Here, we use the property that $x\log(1+x)$ is convex as in [51], and approximate (47), (49), (51), (53) without additional slack variables. Since $a_{k_t} \geq 0$, the constraint (47) can be rewritten as

$$a_{k_t}\log\left(1+a_{k_t}\right) \geq a_{k_t}\alpha_{k_t}\log 2. \tag{65}$$

Its left hand side (LHS) is convex, so we compute the first-order Taylor series approximation of $a_{k_t}\log\left(1+a_{k_t}\right)$ around the point $a_{k_t}^{[n]}$ as

$$\begin{aligned} a_{k_t}\log\left(1+a_{k_t}\right) &\geq a_{k_t}^{[n]}\log\left(1+a_{k_t}^{[n]}\right) + \left(a_{k_t}-a_{k_t}^{[n]}\right) \times\left[\frac{a_{k_t}^{[n]}}{1+a_{k_t}^{[n]}} + \log\left(1+a_{k_t}^{[n]}\right)\right] \\ &= a_{k_t}v_{k_t}^{[n]} - u_{k_t}^{[n]}, \end{aligned} \tag{66}$$

where $v_{k_t}^{[n]}$ and $u_{k_t}^{[n]}$ are expressions of $a_{k_t}^{[n]}$ given by

$$v_{k_t}^{[n]} = \frac{a_{k_t}^{[n]}}{a_{k_t}^{[n]}+1} + \log\left(1+a_{k_t}^{[n]}\right) \quad \text{and} \quad u_{k_t}^{[n]} = \frac{\left(a_{k_t}^{[n]}\right)^2}{a_{k_t}^{[n]}+1}. \tag{67}$$

Now, (65) can be rewritten by $a_{k_t}v_{k_t}^{[n]} - u_{k_t}^{[n]} \geq a_{k_t}\alpha_{k_t}\log 2$, which is SOC representable as

$$\left\|\left[a_{k_t} + \alpha_{k_t}\log 2 - v_{k_t}^{[n]} \quad 2\sqrt{u_{k_t}^{[n]}}\right]\right\|_2 \leq a_{k_t} - \alpha_{k_t}\log 2 + v_{k_t}^{[n]}. \tag{68}$$

Similarly, the constraint (49), (51), (53) can be replaced by (69), (70) and (71), shown at the bottom of the next page. The expressions of $\bar{v}_{k_s}^{[n]}$, $\bar{u}_{k_s}^{[n]}$, $v_{c,k_t}^{[n]}$, $u_{c,k_t}^{[n]}$, $\bar{v}_{c,k_s}^{[n]}$, $\bar{u}_{c,k_s}^{[n]}$ are respectively

$$\begin{aligned} \bar{v}_{k_s}^{[n]} &= \frac{b_{k_s}^{[n]}}{b_{k_s}^{[n]}+1} + \log\left(1+b_{k_s}^{[n]}\right) \text{ and } \bar{u}_{k_s}^{[n]} = \frac{\left(b_{k_s}^{[n]}\right)^2}{b_{k_s}^{[n]}+1}, \\ v_{c,k_t}^{[n]} &= \frac{a_{c,k_t}^{[n]}}{a_{c,k_t}^{[n]}+1} + \log\left(1+a_{c,k_t}^{[n]}\right) \text{ and } u_{c,k_t}^{[n]} = \frac{\left(a_{c,k_t}^{[n]}\right)^2}{a_{c,k_t}^{[n]}+1}, \\ \bar{v}_{c,k_s}^{[n]} &= \frac{b_{c,k_s}^{[n]}}{b_{c,k_s}^{[n]}+1} + \log\left(1+b_{c,k_s}^{[n]}\right) \text{ and } \bar{u}_{c,k_s}^{[n]} = \frac{\left(b_{c,k_s}^{[n]}\right)^2}{b_{c,k_s}^{[n]}+1}. \end{aligned} \tag{72}$$

By replacing the constraints (45)-(52) with (55), (58), (59), (60), (66)-(69), we obtain

$$\begin{aligned}\mathcal{A}_1: \quad & \max_{q,\mathbf{W},\mathbf{P},\mathbf{c}^{sat},\mathbf{c}^{bs},\mathbf{r},\boldsymbol{\alpha},\mathbf{a},\mathbf{a}_c,\mathbf{b},\mathbf{b}_c} \quad q \\ & s.t.\ (57),(61),(68),(70), \quad \forall k_t \in \mathcal{K}_t \\ & \quad (60),(62),(69),(71), \quad \forall k_s \in \mathcal{K}_s \\ & \quad (36),(37),(39),(40),(42),(44)\end{aligned} \tag{73}$$

The n-th iteration of the problem $\mathcal{A}_1$ belongs to SOCP and can be efficiently solved by the standard solvers in CVX. In each iteration, the problem defined around the solution of the previous iteration is solved. Variables are updated iteratively until a stopping criterion is satisfied. We summarize the procedure of this RSMA-based joint beamforming scheme in Algorithm 1. ε is the tolerance value. The optimal solution of Problem $\mathcal{A}_1$ at iteration-n is a feasible solution of the problem at iteration-$n+1$. As a consequence, the objective variable q increases monotonically. It is bounded above by the transmit power constraints. The proposed Algorithm 1 is guaranteed to converge while the global optimality of the achieved solution can not be guaranteed. The solution of the proposed SCA-based algorithm converges to the set of KKT points (which is also known as the stationary points) of problem $\mathcal{P}_1$ [52].

Algorithm 1 Proposed Joint Beamforming Scheme

Initialize: $n \leftarrow 0,\ \mathbf{W}^{[n]}, \mathbf{P}^{[n]}, \mathbf{a}^{[n]}, \mathbf{a}_c^{[n]}, \mathbf{b}^{[n]}, \mathbf{b}_c^{[n]}, q^{[n]}$;
repeat
Solve $\mathcal{A}_1$ at $\left(\mathbf{W}^{[n]}, \mathbf{P}^{[n]}, \mathbf{a}^{[n]}, \mathbf{a}_c^{[n]}, \mathbf{b}^{[n]}, \mathbf{b}_c^{[n]}\right)$ to get the optimal solution $\left(\breve{\mathbf{W}}, \breve{\mathbf{P}}, \breve{\mathbf{a}}, \breve{\mathbf{a}}_c, \breve{\mathbf{b}}, \breve{\mathbf{b}}_c, \breve{q}\right)$;
$n \leftarrow n+1$;
Update $\mathbf{W}^{[n]} \leftarrow \breve{\mathbf{W}}, \mathbf{P}^{[n]} \leftarrow \breve{\mathbf{P}}, \mathbf{a}^{[n]} \leftarrow \breve{\mathbf{a}}, \mathbf{a}_c^{[n]} \leftarrow \breve{\mathbf{a}}_c, \mathbf{b}^{[n]} \leftarrow \breve{\mathbf{b}}, \mathbf{b}_c^{[n]} \leftarrow \breve{\mathbf{b}}_c, q^{[n]} \leftarrow \breve{q}$;
until $\left|q^{[n]} - q^{[n-1]}\right| < \varepsilon$;

B. Joint Beamforming Design for Cooperative STIN

When RSMA-based *cooperative STIN* is considered, the optimization problem of max-min rate fairness among all users is given by

$$\mathcal{P}_2: \quad \max_{\acute{\mathbf{W}},\acute{\mathbf{P}},\acute{\mathbf{c}}} \ \min_{n_s\in\mathcal{N}_s,k_t\in\mathcal{K}_t} \ \left\{\acute{R}_{k_t}^{bs}, \acute{R}_{k_s}^{sat}\right\} \tag{74}$$

$$s.t.\ \acute{R}_{c,k_t}^{bs} \geq \sum_{j=1}^{K_t} \acute{C}_j^{bs} + \sum_{j=1}^{N_s} \acute{C}_j^{sat}, \quad \forall k_t \in \mathcal{K}_t \tag{75}$$

$$\acute{C}_{k_t}^{bs} \geq 0 \quad \forall k_t \in \mathcal{K}_t \tag{76}$$

$$\mathrm{tr}\left(\acute{\mathbf{P}}\acute{\mathbf{P}}^H\right) \leq P_t \tag{77}$$

$$\acute{R}_{c,k_s}^{sat} \geq \sum_{j=1}^{K_t} \acute{C}_j^{bs} + \sum_{j=1}^{N_s} \acute{C}_j^{sat}, \quad \forall k_s \in \mathcal{K}_s \tag{78}$$

$$\acute{C}_{n_s}^{sat} \geq 0, \quad \forall n_s \in \mathcal{N}_s \tag{79}$$

$$\left(\acute{\mathbf{W}}\acute{\mathbf{W}}^H\right)_{n_s,n_s} \leq \frac{P_s}{N_s}, \quad \forall n_s \in \mathcal{N}_s \tag{80}$$

where $\acute{\mathbf{c}} = [\acute{C}_1^{sat}, \cdots, \acute{C}_{N_s}^{sat}, \acute{C}_1^{bs}, \cdots, \acute{C}_{K_t}^{bs}]^T$ is the vector of all common rate portions. (75) and (78) guarantee that the common stream of the whole system $\acute{s}_c$ can be decoded by all SUs and CUs. (76) and (79) ensure non-negativity of each element in $\acute{\mathbf{c}}$. (77) and (80) are respectively the sum transmit power constraint of the BS and per-feed transmit power constraints of the satellite. The formulated MMF problem for *cooperative STIN* is also non-convex. Note that the main difference between $\mathcal{P}_1$ and $\mathcal{P}_2$ lies in the transmit data information sharing in $\mathcal{P}_2$. One super common stream is transmitted at both the satellite and BS instead of transmitting individual common streams. The achievable rate expressions and beamforming matrices of *cooperative STIN* have been given in Section III. We can still use the SCA-based algorithm to solve $\mathcal{P}_2$. Here, we omit the detailed problem transformation and optimization framework, which follow the same procedure as that for $\mathcal{P}_1$.

IV. Robust Joint Beamforming Scheme

In this section, we further investigate the beamforming design for RSMA-based *coordinated STIN* and *cooperative STIN* considering satellite channel phase uncertainty. The CSIT of terrestrial channels is assumed to be perfect. From the satellite channel model given in Section II, we can observe that the amplitudes of the channel vector components are determined by some constant coefficients during the coherence time interval, including the free space loss, satellite antenna gain and rain attenuation [17]. However, the satellite channel phases vary rapidly due to a series of time-varying factors, such as the use of different local oscillators (LO) onboard, the rain, cloud and gaseous absorption, and the use of low-noise block (LNB) at receivers [17], [19]. Therefore, within a coherence time interval, the phase of the channel vector from the satellite to SU-k_s at time instant t_1 can be modeled as

$$\boldsymbol{\phi}_{k_s}(t_1) = \boldsymbol{\phi}_{k_s}(t_0) + \mathbf{e}_{k_s}, \tag{81}$$

$$\left\| \left[b_{k_s} + r_{k_s}\log 2 - \bar{v}_{k_s}^{[n]} \quad 2\sqrt{\bar{u}_{k_s}^{[n]}} \right] \right\|_2 \leq b_{k_s} - r_{k_s}\log 2 + \bar{v}_{k_s}^{[n]}, \tag{69}$$

$$\left\| \left[a_{c,k_t} + \sum_{j=1}^{K_t} C_j^{bs}\log 2 - v_{c,k_t}^{[n]} \quad 2\sqrt{u_{c,k_t}^{[n]}} \right] \right\|_2 \leq a_{c,k_t} - \sum_{j=1}^{K_t} C_j^{bs}\log 2 + v_{c,k_t}^{[n]}, \tag{70}$$

$$\left\| \left[b_{c,k_s} + \sum_{j=1}^{N_s} C_j^{sat}\log 2 - \bar{v}_{c,k_s}^{[n]} \quad 2\sqrt{\bar{u}_{c,k_s}^{[n]}} \right] \right\|_2 \leq b_{c,k_s} - \sum_{j=1}^{N_s} C_j^{sat}\log 2 + \bar{v}_{c,k_s}^{[n]}. \tag{71}$$

where $\boldsymbol{\phi}_{k_s}(t_0)$ represents the phase vector, which is estimated at the previous time instant t_0 and fed back to the GW. $\mathbf{e}_{k_s} = [e_{k_s,1}, e_{k_s,2}, \cdots, e_{k_s,N_s}]^T$ is the phase uncertainty following the distribution $\mathbf{e}_{k_s} \sim \mathcal{N}(\mathbf{0}, \delta^2\mathbf{I})$, with i.i.d Gaussian random entries. For ease of notation, we can generally indicate $\boldsymbol{\phi}_{k_s}(t_1)$ and $\boldsymbol{\phi}_{k_s}(t_0)$ by $\boldsymbol{\phi}_{k_s}$ and $\widehat{\boldsymbol{\phi}}_{k_s}$ respectively. Since we assume constant channel amplitudes within the coherence time interval, the channel vector from the satellite to SU-k_s can be written as

$$\mathbf{f}_{k_s} = \widehat{\mathbf{f}}_{k_s} \circ \mathbf{x}_{k_s} = \operatorname{diag}\big(\widehat{\mathbf{f}}_{k_s}\big)\mathbf{x}_{k_s}, \tag{82}$$

where $\mathbf{x}_{k_s} = \exp\{j\mathbf{e}_{k_s}\}$ is a random vector. We further assume that the channel estimate $\widehat{\mathbf{f}}_{k_s}$ and the correlation matrix of $\mathbf{x}_{k_s}$ denoted by $\mathbf{X}_{k_s} = \mathbb{E}\{\mathbf{x}_{k_s}\mathbf{x}_{k_s}^H\}$ are known at the GW [17]. For the interfering channels, by defining $\mathbf{y}_{k_t} = \exp\{j\mathbf{e}'_{k_t}\}$ and $\mathbf{e}'_{k_t} = \left[e'_{k_t,1}, e'_{k_t,2}, \cdots, e'_{k_t,N_s}\right]^T$ following $\mathbf{e}'_{k_t} \sim \mathcal{N}(\mathbf{0}, \delta^2\mathbf{I})$, the channel vector from the satellite to CU-k_t write as

$$\mathbf{z}_{k_t} = \widehat{\mathbf{z}}_{k_t} \circ \mathbf{y}_{k_t} = \operatorname{diag}\big(\widehat{\mathbf{z}}_{k_t}\big)\mathbf{y}_{k_t}, \tag{83}$$

where the channel estimate $\widehat{\mathbf{z}}_{k_t}$ and the correlation matrix $\mathbf{Y}_{k_t} = \mathbb{E}\{\mathbf{y}_{k_t}\mathbf{y}_{k_t}^H\}$ are available at the GW. Hence, we concentrate on the expectation-based robust beamforming design. The MMF optimization problem for RSMA-based *coordinated STIN* considering satellite phase uncertainty remains the same as $\mathcal{P}_1$ in Section III, By introducing auxiliary variables q, $\boldsymbol{\alpha} = [\alpha_1, \cdots, \alpha_{K_t}]^T$, $\mathbf{r} = [r_1, \cdots, r_{K_s}]^T$, $W = \{\mathbf{W}_c, \mathbf{W}_1, \cdots, \mathbf{W}_{N_s}\}$ and $P = \{\mathbf{P}_c, \mathbf{P}_1, \cdots, \mathbf{P}_{K_t}\}$, the original $\mathcal{P}_1$ can be equivalently transformed into a semi-definite programming (SDP) form with rank-one constraints

$$\mathcal{D}_1: \quad \max_{W,P,\mathbf{c}^{sat},\mathbf{c}^{bs},q,\mathbf{r},\boldsymbol{\alpha}} \ q \tag{84}$$

$$s.t.\ \operatorname{tr}(\mathbf{P}_c) + \sum_{k_t=1}^{K_t} \operatorname{tr}(\mathbf{P}_{k_t}) \le P_t \tag{85}$$

$$\big[\mathbf{W}_c + \sum_{i=1}^{N_s} \mathbf{W}_i\big]_{n_s,n_s} \le \frac{P_s}{N_s}, \quad n_s \in \mathcal{N}_s \tag{86}$$

$$\mathbf{W}_c \succeq 0,\ \mathbf{W}_{n_s} \succeq 0, \quad \forall n_s \in \mathcal{N}_s \tag{87}$$

$$\mathbf{P}_c \succeq 0,\ \mathbf{P}_{k_t} \succeq 0, \quad \forall k_t \in \mathcal{K}_t \tag{88}$$

$$\operatorname{rank}(\mathbf{W}_c) = 1, \quad \operatorname{rank}(\mathbf{W}_{n_s}) = 1, \quad \forall n_s \in \mathcal{N}_s \tag{89}$$

$$\operatorname{rank}(\mathbf{P}_c) = 1, \quad \operatorname{rank}(\mathbf{P}_{k_t}) = 1, \quad \forall k_t \in \mathcal{K}_t \tag{90}$$

$$(35), (36), (38), (39), (42) - (45)$$

where $\mathbf{W}_c = \mathbf{w}_c\mathbf{w}_c^H$, $\{\mathbf{W}_{n_s} = \mathbf{w}_{n_s}\mathbf{w}_{n_s}^H\}_{n_s=1}^{N_s}$, $\mathbf{P}_c = \mathbf{p}_c\mathbf{p}_c^H$, $\{\mathbf{P}_{k_t} = \mathbf{p}_{k_t}\mathbf{p}_{k_t}^H\}_{k_t=1}^{K_t}$. (85) and (86) are transmit power constraints. All the rate expressions in this section are redefined by the ergodic form $R \triangleq \mathbb{E}\{\log_2(1+\mathrm{SINR})\}$, as the metric of average robust design. By taking (45) as an example, $R_{k_s}^{sat}$ can be approximated by (91), shown at the bottom of the page. Note that (91) is very tight and has been verified to be theoretically accurate in [53]. Specifically, $\mathbf{F}_{k_s} = \operatorname{diag}\big(\widehat{\mathbf{f}}_{k_s}\big)\mathbf{x}_{k_s}\mathbf{x}_{k_s}^H\operatorname{diag}\big(\widehat{\mathbf{f}}_{k_s}^H\big)$. $\overline{\mathbf{F}}_{k_s} = \mathbb{E}\{\mathbf{F}_{k_s}\} = \operatorname{diag}\big(\widehat{\mathbf{f}}_{k_s}\big)\mathbf{X}_{k_s}\operatorname{diag}\big(\widehat{\mathbf{f}}_{k_s}^H\big)$ is defined as the channel correlation matrix, which captures the expectation over the distribution of phase uncertainty. Based on the approximated rate expressions, $\mathcal{D}_1$ can be rewritten as $\mathcal{F}_1$. η and ξ are the sets of introduced slack variables. The constraints (93)-(95), (96)-(98), (99)-(101), and (102)-(104), shown at the bottom of the next page, are respectively the expansions of the rate constraints (43), (45), (35) and (38). Note that (95), (98), (101) and (104) are non-convex with convex LHSs, which can be approximated by the first-order Taylor approximation. Hence, we obtain the approximated linear constraints (105) - (108), shown at the bottom of the next page, where n represents the n-th SCA iteration. The constraints (95), (98), (101) and (104) belong to generalized nonlinear convex program with high computational complexity. Following the same method introduced in Section III, they can be represented in linear and SOC forms (109) - (116), shown at the bottom of page 12.

Since rank-one implies only one nonzero eigenvalue, the non-convex constraints (89) and (90) can be rewritten by

$$\begin{aligned} &\operatorname{tr}(\mathbf{W}_c) - \lambda_{\max}(\mathbf{W}_c) = 0, \\ &\operatorname{tr}(\mathbf{W}_{n_s}) - \lambda_{\max}(\mathbf{W}_{n_s}) = 0, \quad \forall n_s \in \mathcal{N}_s, \end{aligned} \tag{117}$$

$$\begin{aligned} &\operatorname{tr}(\mathbf{P}_c) - \lambda_{\max}(\mathbf{P}_c) = 0, \\ &\operatorname{tr}(\mathbf{P}_{k_t}) - \lambda_{\max}(\mathbf{P}_{k_t}) = 0, \quad \forall k_t \in \mathcal{K}_t, \end{aligned} \tag{118}$$

where $\lambda_{\max}(\mathbf{X})$ denotes the maximum eigenvalue of $\mathbf{X} \succeq 0$. Then, we build a penalty function to insert these constraints into the objective function (92), shown at the bottom of the next page, and obtain (119), shown at the bottom of page 12. β is a proper penalty factor to guarantee the penalty function as small as possible. (119) is nonconcave due to the existence of the penalty function. To tackle this issue, we adopt an iterative method [18]. By taking $\operatorname{tr}(\mathbf{W}_c) - \lambda_{\max}(\mathbf{W}_c)$ as an example, we have the following inequality

$$\begin{aligned} &\operatorname{tr}(\mathbf{W}_c) - (\mathbf{v}_{c,\max}^{[n]})^H\mathbf{W}_c\mathbf{v}_{c,\max}^{[n]} \\ &\quad \ge \operatorname{tr}(\mathbf{W}_c) - \lambda_{\max}(\mathbf{W}_c) \ge 0, \end{aligned} \tag{121}$$

$$\begin{aligned} R_{k_s}^{sat} &= \mathbb{E}\left\{\log_2\left(1+\gamma_{k_s}^{sat}\right)\right\} \\ &\approx \log_2\left(\frac{\mathbb{E}\left\{\operatorname{tr}\left(\mathbf{F}_{k_s}\mathbf{W}_{\mu(k_s)}\right)\right\} + \sum_{i=1,i\neq\mu(k_s)}^{N_s}\mathbb{E}\left\{\operatorname{tr}\left(\mathbf{F}_{k_s}\mathbf{W}_i\right)\right\} + \sigma_{k_s}^{sat2}}{\sum_{i=1,i\neq\mu(k_s)}^{N_s}\mathbb{E}\left\{\operatorname{tr}\left(\mathbf{F}_{k_s}\mathbf{W}_i\right)\right\} + \sigma_{k_s}^{sat2}}\right) \\ &= \log_2\left(\frac{\operatorname{tr}\left(\overline{\mathbf{F}}_{k_s}\mathbf{W}_{\mu(k_s)}\right) + \sum_{i=1,i\neq\mu(k_s)}^{N_s}\operatorname{tr}\left(\overline{\mathbf{F}}_{k_s}\mathbf{W}_i\right) + \sigma_{k_s}^{sat2}}{\sum_{i=1,i\neq\mu(k_s)}^{N_s}\operatorname{tr}\left(\overline{\mathbf{F}}_{k_s}\mathbf{W}_i\right) + \sigma_{k_s}^{sat2}}\right). \end{aligned} \tag{91}$$

where $\mathbf{v}_{c,\max}$ is the normalized eigenvector corresponding to the maximum eigenvalue $\lambda_{\max}(\mathbf{W}_c)$. Furthermore, we define $\mathbf{v}_{n_s,\max}$ as the corresponding eigenvector of $\lambda_{\max}(\mathbf{W}_{n_s})$, and so does $\mathbf{b}_{c,\max}$ for $\lambda_{\max}(\mathbf{P}_c)$ and $\mathbf{b}_{k_t,\max}$ for $\lambda_{\max}(\mathbf{P}_{k_t})$. Let PF denote the iterative penalty function, which is given by (120), shown at the bottom of the next page. Eventually, the approximate problem at iteration-n is given by

$$\mathcal{G}_1: \max_{W,P,\mathbf{c}^{sat},\mathbf{c}^{bs},q,\mathbf{r},\alpha,\eta,\xi,t} q - \mathrm{PF}$$
$$s.t.\ (36),(39),(42),(44),(85)-(88),(93),(96),(99),(102)$$
$$(105),(107),(109),(110),(113),(114),\ \forall k_t \in \mathcal{K}_t$$
$$(106),(108),(111),(112),(115),(116),\ \forall k_s \in \mathcal{K}_s \quad (122)$$

The problem is convex involving only linear matrix inequality (LMI) and SOC constraints, and can be effectively solved by CVX. In each iteration, the problem defined around the solution of the previous iteration is solved. We summarize

$$\mathcal{F}_1: \max_{W,P,\mathbf{c}^{sat},\mathbf{c}^{bs},q,\mathbf{r},\boldsymbol{\alpha},\eta,\xi} q \quad (92)$$
$$s.t.\ \eta_{k_t}^{bs} - \xi_{k_t}^{bs} \geq \alpha_{k_t}\log 2,\ \forall k_t \in \mathcal{K}_t \quad (93)$$
$$e^{\eta_{k_t}^{bs}} \leq \mathrm{tr}(\mathbf{H}_{k_t}\mathbf{P}_{k_t}) + \sum_{j=1,j\neq k_t}^{K_t}\mathrm{tr}(\mathbf{H}_{k_t}\mathbf{P}_j) + \mathrm{tr}(\overline{\mathbf{Z}}_{k_t}\mathbf{W}_c) + \sum_{i=1}^{N_s}\mathrm{tr}(\overline{\mathbf{Z}}_{k_t}\mathbf{W}_i) + \sigma_{k_t}^{bs2},\ \forall k_t \in \mathcal{K}_t \quad (94)$$
$$e^{\xi_{k_t}^{bs}} \geq \sum_{j=1,j\neq k_t}^{K_t}\mathrm{tr}(\mathbf{H}_{k_t}\mathbf{P}_j) + \mathrm{tr}(\overline{\mathbf{Z}}_{k_t}\mathbf{W}_c) + \sum_{i=1}^{N_s}\mathrm{tr}(\overline{\mathbf{Z}}_{k_t}\mathbf{W}_i) + \sigma_{k_t}^{bs2},\ \forall k_t \in \mathcal{K}_t \quad (95)$$
$$\eta_{k_s}^{sat} - \xi_{k_s}^{sat} \geq r_{k_s}\log 2,\ \forall k_s \in \mathcal{K}_s \quad (96)$$
$$e^{\eta_{k_s}^{sat}} \leq \mathrm{tr}(\overline{\mathbf{F}}_{k_s}\mathbf{W}_{\mu(k_s)}) + \sum_{i=1,i\neq\mu(k_s)}^{N_s}\mathrm{tr}(\overline{\mathbf{F}}_{k_s}\mathbf{W}_i) + \sigma_{k_s}^{sat2},\ \forall k_s \in \mathcal{K}_s \quad (97)$$
$$e^{\xi_{k_s}^{sat}} \geq \sum_{i=1,i\neq\mu(k_s)}^{N_s}\mathrm{tr}(\overline{\mathbf{F}}_{k_s}\mathbf{W}_i) + \sigma_{k_s}^{sat2},\ \forall k_s \in \mathcal{K}_s \quad (98)$$
$$\eta_{c,k_t}^{bs} - \xi_{c,k_t}^{bs} \geq \sum_{j=1}^{K_t} C_j^{bs}\log 2,\ \forall k_t \in \mathcal{K}_t \quad (99)$$
$$e^{\eta_{c,k_t}^{bs}} \leq \mathrm{tr}(\mathbf{H}_{k_t}\mathbf{P}_c) + \sum_{j=1}^{K_t}\mathrm{tr}(\mathbf{H}_{k_t}\mathbf{P}_j) + \mathrm{tr}(\overline{\mathbf{Z}}_{k_t}\mathbf{W}_c) + \sum_{i=1}^{N_s}\mathrm{tr}(\overline{\mathbf{Z}}_{k_t}\mathbf{W}_i) + \sigma_{k_t}^{bs2},\ \forall k_t \in \mathcal{K}_t \quad (100)$$
$$e^{\xi_{c,k_t}^{bs}} \geq \sum_{j=1}^{K_t}\mathrm{tr}(\mathbf{H}_{k_t}\mathbf{P}_j) + \mathrm{tr}(\overline{\mathbf{Z}}_{k_t}\mathbf{W}_c) + \sum_{i=1}^{N_s}\mathrm{tr}(\overline{\mathbf{Z}}_{k_t}\mathbf{W}_i) + \sigma_{k_t}^{bs2},\ \forall k_t \in \mathcal{K}_t \quad (101)$$
$$\eta_{c,k_s}^{sat} - \xi_{c,k_s}^{sat} \geq \sum_{j=1}^{N_s} C_j^{sat}\log 2,\ \forall k_s \in \mathcal{K}_s \quad (102)$$
$$e^{\eta_{c,k_s}^{sat}} \leq \mathrm{tr}(\overline{\mathbf{F}}_{k_s}\mathbf{W}_c) + \sum_{i=1}^{N_s}\mathrm{tr}(\overline{\mathbf{F}}_{k_s}\mathbf{W}_i) + \sigma_{k_s}^{sat2},\ \forall k_s \in \mathcal{K}_s \quad (103)$$
$$e^{\xi_{c,k_s}^{sat}} \geq \sum_{i=1}^{N_s}\mathrm{tr}(\overline{\mathbf{F}}_{k_s}\mathbf{W}_i) + \sigma_{k_s}^{sat2},\ \forall k_s \in \mathcal{K}_s \quad (104)$$
$$(36),(39),(42),(44),(85)-(90)$$

$$\sum_{j=1,j\neq k_t}^{K_t}\mathrm{tr}(\mathbf{H}_{k_t}\mathbf{P}_j) + \mathrm{tr}(\overline{\mathbf{Z}}_{k_t}\mathbf{W}_c) + \sum_{i=1}^{N_s}\mathrm{tr}(\overline{\mathbf{Z}}_{k_t}\mathbf{W}_i) + \sigma_{k_t}^{bs2} \leq e^{\xi_{k_t}^{bs[n]}}\left(\xi_{k_t}^{bs} - \xi_{k_t}^{bs[n]} + 1\right), \quad (105)$$
$$\sum_{i=1,i\neq\mu(k_s)}^{N_s}\mathrm{tr}(\overline{\mathbf{F}}_{k_s}\mathbf{W}_i) + \sigma_{k_s}^{sat2} \leq e^{\xi_{k_s}^{sat[n]}}\left(\xi_{k_s}^{sat} - \xi_{k_s}^{sat[n]} + 1\right), \quad (106)$$
$$\sum_{j=1}^{K_t}\mathrm{tr}(\mathbf{H}_{k_t}\mathbf{P}_j) + \mathrm{tr}(\overline{\mathbf{Z}}_{k_t}\mathbf{W}_c) + \sum_{i=1}^{N_s}\mathrm{tr}(\overline{\mathbf{Z}}_{k_t}\mathbf{W}_i) + \sigma_{k_t}^{bs2} \leq e^{\xi_{c,k_t}^{bs[n]}}\left(\xi_{c,k_t}^{bs} - \xi_{c,k_t}^{bs[n]} + 1\right), \quad (107)$$
$$\sum_{i=1}^{N_s}\mathrm{tr}(\overline{\mathbf{F}}_{k_s}\mathbf{W}_i) + \sigma_{k_s}^{sat2} \leq e^{\xi_{c,k_s}^{sat[n]}}\left(\xi_{c,k_s}^{sat} - \xi_{c,k_s}^{sat[n]} + 1\right). \quad (108)$$

the procedure of this robust joint beamforming scheme in Algorithm 2. Finally, eigenvalue decomposition (EVD) can be used to obtain the optimized beamforming vectors. The optimal solution $(W^{[n]}, P^{[n]}, \eta^{[n]}, \xi^{[n]}, t^{[n]})$ of the n-th iteration is a feasible solution of the $(n+1)$-th iteration. Thus, such algorithm generates a nondecreasing sequence of objective values, which are bounded above by the transmit power constraints. Moreover, the objective function is guaranteed to converge by the existence of lower bounds, i.e., (121). In other words, the rank-one constraints can be satisfied [18]. The obtained solution satisfies the KKT optimality conditions of $\mathcal{G}_1$, which are indeed identical to those of $\mathcal{D}_1$ at convergence [52]. However, the global optimality of the achieved solution can not be guaranteed. The MMF optimization problem of RSMA-based *cooperative STIN* considering satellite phase uncertainty remains the same as $\mathcal{P}_2$ in Section III. Here, we still omit the detailed optimization framework. The process keeps the same as that for the *coordinated STIN*.

Remark 2: Recall that the problem formulations in Algorithm 1 and Algorithm 2 involve only SOC and LMI constraints. They both can be efficiently solved by using standard interior-point method (IPM). It suggests that the worst-case runtime can be used to compare the computational complexities of different problems [54]. Hence, the worst-case computational complexity of the proposed joint beamforming scheme in Algorithm 1 and the robust joint beamforming scheme in Algorithm 2 are respectively $\mathcal{O}\Big([N_s^2 + N_t K_t]^{3.5} \log\left(\varepsilon^{-1}\right)\Big)$ *and* $\mathcal{O}\Big([N_s^3 + N_t^2 K_t]^{3.5} \log\left(\varepsilon^{-1}\right)\Big)$ *[49], [55], where* ε *is the convergence tolerance. Similarly, the complexity of the cooperative STIN scenarios of Algorithm 1 and Algorithm 2 are respectively* $\mathcal{O}\Big([N_s\left(N_s+K_t\right)+N_t\left(N_s+K_t\right)]^{3.5} \log\left(\varepsilon^{-1}\right)\Big)$ *and* $\mathcal{O}\Big([N_s^2\left(N_s+K_t\right)+N_t^2\left(N_s+K_t\right)]^{3.5} \log\left(\varepsilon^{-1}\right)\Big)$*, which are higher than the coordinated STIN scenarios because of the larger number of variables in precoder design.*

V. Simulation Results

In this section, simulation results are provided to evaluate the performance of the proposed joint beamforming algorithms. Both perfect CSIT and imperfect CSIT with satellite channel phase uncertainties are considered. The tolerance of accuracy is set to be $\varepsilon = 10^{-4}$. Channel models have been

$$t_{k_t}^{bs} \le \mathrm{tr}\left(\mathbf{H}_{k_t}\mathbf{P}_{k_t}\right) + \sum_{j=1, j\neq k_t}^{K_t} \mathrm{tr}\left(\mathbf{H}_{k_t}\mathbf{P}_{j}\right) + \mathrm{tr}\left(\overline{\mathbf{Z}}_{k_t}\mathbf{W}_c\right) + \sum_{i=1}^{N_s} \mathrm{tr}\left(\overline{\mathbf{Z}}_{k_t}\mathbf{W}_i\right) + \sigma_{k_t}^{bs2}, \tag{109}$$

$$\left\| t_{k_t}^{bs} + \eta_{k_t}^{bs} - \left(\log(t_{k_t}^{bs[n]}) + 1\right) \quad 2\sqrt{t_{k_t}^{bs[n]}} \right\|_2 \le t_{k_t}^{bs} - \eta_{k_t}^{bs} + \left(\log(t_{k_t}^{bs[n]}) + 1\right), \tag{110}$$

$$t_{k_s}^{sat} \le \mathrm{tr}\left(\overline{\mathbf{F}}_{k_s}\mathbf{W}_{\mu(k_s)}\right) + \sum_{i=1, i\neq\mu(k_s)}^{N_s} \mathrm{tr}\left(\overline{\mathbf{F}}_{k_s}\mathbf{W}_i\right) + \sigma_{k_s}^{sat2}, \tag{111}$$

$$\left\| t_{k_s}^{sat} + \eta_{k_s}^{sat} - \left(\log(t_{k_s}^{sat[n]}) + 1\right) \quad 2\sqrt{t_{k_s}^{sat[n]}} \right\|_2 \le t_{k_s}^{sat} - \eta_{k_s}^{sat} + \left(\log(t_{k_s}^{sat[n]}) + 1\right), \tag{112}$$

$$t_{c,k_t}^{bs} \le \mathrm{tr}\left(\mathbf{H}_{k_t}\mathbf{P}_{c}\right) + \sum_{j=1}^{K_t} \mathrm{tr}\left(\mathbf{H}_{k_t}\mathbf{P}_{j}\right) + \mathrm{tr}\left(\overline{\mathbf{Z}}_{k_t}\mathbf{W}_c\right) + \sum_{i=1}^{N_s} \mathrm{tr}\left(\overline{\mathbf{Z}}_{k_t}\mathbf{W}_i\right) + \sigma_{k_t}^{bs2}, \tag{113}$$

$$\left\| t_{c,k_t}^{bs} + \eta_{c,k_t}^{bs} - \left(\log(t_{c,k_t}^{bs[n]}) + 1\right) \quad 2\sqrt{t_{c,k_t}^{bs[n]}} \right\|_2 \le t_{c,k_t}^{bs} - \eta_{c,k_t}^{bs} + \left(\log(t_{c,k_t}^{bs[n]}) + 1\right), \tag{114}$$

$$t_{c,k_s}^{sat} \le \mathrm{tr}\left(\overline{\mathbf{F}}_{k_s}\mathbf{W}_{c}\right) + \sum_{i=1}^{N_s} \mathrm{tr}\left(\overline{\mathbf{F}}_{k_s}\mathbf{W}_i\right) + \sigma_{k_s}^{sat2}, \tag{115}$$

$$\left\| t_{c,k_s}^{sat} + \eta_{c,k_s}^{sat} - \left(\log(t_{c,k_s}^{sat[n]}) + 1\right) \quad 2\sqrt{t_{c,k_s}^{sat[n]}} \right\|_2 \le t_{c,k_s}^{sat} - \eta_{c,k_s}^{sat} + \left(\log(t_{c,k_s}^{sat[n]}) + 1\right). \tag{116}$$

$$\begin{aligned} \max_{W,P,\mathbf{c}^{sat},\mathbf{c}^{bs},q,\mathbf{r},\alpha,\eta,\xi} \; & q - \beta\Big(\left[\mathrm{tr}\left(\mathbf{W}_c\right) - \lambda_{\max}\left(\mathbf{W}_c\right)\right] + \sum_{n_s=1}^{N_s} \left[\mathrm{tr}\left(\mathbf{W}_{n_s}\right) - \lambda_{\max}\left(\mathbf{W}_{n_s}\right)\right] \\ & + \left[\mathrm{tr}\left(\mathbf{P}_c\right) - \lambda_{\max}\left(\mathbf{P}_c\right)\right] + \sum_{k_t=1}^{K_t} \left[\mathrm{tr}\left(\mathbf{P}_{k_t}\right) - \lambda_{\max}\left(\mathbf{P}_{k_t}\right)\right] \Big). \end{aligned} \tag{119}$$

$$\begin{aligned} \mathrm{PF} = \beta\Big(& \left[\mathrm{tr}\left(\mathbf{W}_c\right) - \left(\mathbf{v}_{c,\max}^{[n]}\right)^H \mathbf{W}_c \mathbf{v}_{c,\max}^{[n]}\right] + \sum_{n_s=1}^{N_s} \left[\mathrm{tr}\left(\mathbf{W}_{n_s}\right) - \left(\mathbf{v}_{n_s,\max}^{[n]}\right)^H \mathbf{W}_{n_s} \mathbf{v}_{n_s,\max}^{[n]}\right] \\ & + \left[\mathrm{tr}\left(\mathbf{P}_c\right) - \left(\mathbf{b}_{c,\max}^{[n]}\right)^H \mathbf{P}_c \mathbf{b}_{c,\max}^{[n]}\right] + \sum_{k_t=1}^{K_t} \left[\mathrm{tr}\left(\mathbf{P}_{k_t}\right) - \left(\mathbf{b}_{k_t,\max}^{[n]}\right)^H \mathbf{P}_c \mathbf{b}_{k_t,\max}^{[n]}\right] \Big). \end{aligned} \tag{120}$$

Algorithm 2 Robust Joint Beamforming Scheme

Initialize: $n \leftarrow 0, W^{[n]}, P^{[n]}, \eta^{[n]}, \xi^{[n]}, t^{[n]}$;
repeat
Solve $\mathcal{G}_1$ at $(W^{[n]}, P^{[n]}, \eta^{[n]}, \xi^{[n]}, t^{[n]})$ to get the optimal solution $(\breve{W}, \breve{P}, \breve{\eta}, \breve{\xi}, \breve{t}, \breve{\text{objective}})$;
$n \leftarrow n+1$;
Update $W^{[n]} \leftarrow \breve{W}, P^{[n]} \leftarrow \breve{P}, \eta^{[n]} \leftarrow \breve{\eta}, \xi^{[n]} \leftarrow \breve{\xi}, t^{[n]} \leftarrow \breve{t}, \text{objective}^{[n]} \leftarrow \breve{\text{objective}}$;
until $\left|\text{objective}^{[n]} - \text{objective}^{[n-1]}\right| < \varepsilon$;

TABLE I
SIMULATION PARAMETERS

Parameter	Value
Frequency band (carrier frequency)	Ka (28 GHz)
Satellite height	35786 km (GEO)
Bandwidth	500 MHz
3 dB angle	0.4°
Maximum beam gain	52 dBi
User terminal antenna gain	42.7 dBi
Rain fading parameters	$(\mu, \sigma) = (-3.125, 1.591)$
UPA inter-element spacing	$d_1 = d_2 = \frac{\lambda}{2}$
Number of NLoS paths	3

introduced in Section II, and the simulation parameters are listed in Table I [42], [56]. The satellite is equipped with N_s antennas. ρ multicasting SUs locate uniformly in each beam coverage area. Ideally, user scheduling can be optimized together with the beamforming design, however, this is out of the scope of this paper. According to the architecture of SFPB, which is popular in modern satellites such as Eutelsat Ka-Sat, the number of SUs is $K_s = \rho N_s$. Meanwhile, the BS is deployed with UPA with N_t antennas. We assume K_t CUs uniformly distributed within the BS coverage. In the satellite channel model, since we normalize the noise power by $\kappa T_{sys} B_w$ in (2), we can claim $\sigma_{k_s}^{sat2} = \sigma_{k_t}^{bs2} = 1$, $\forall k_s \in \mathcal{K}_s$, $\forall k_t \in \mathcal{K}_t$ in the simulations. The transmit SNRs [3] can be read from the transmit power P_s and P_t. All MMF rate curves throughout the simulations are calculated by averaging 100 channel realizations.

At first, we assume that perfect CSI is available at the GW. Fig. 3 compares the MMF rate performance of RSMA-based *coordinated* and *cooperative scheme*. The label "coordinated rsma" means RSMA is adopted at both the satellite and BS, while "cooperative rsma" means the satellite and BS work cooperatively as a super transmitter while RSMA is adopted. As P_t grows, we can see that the MMF rates of both schemes increase and tend to saturate at large P_t region. The *cooperative scheme* outperforms the *coordinated scheme* apparently at low P_t region. The gap between two schemes decreases gradually as P_t grows, and finally converge to the same value when P_t is sufficiently large. The reasons are as follows. When P_t is relatively small, the STIN's performance is restricted in the *coordinated scheme* because the SINRs of CUs are much lower than the SINRs of SUs. Joint beamforming is designed to achieve optimal MMF rates. However, in the *cooperative scheme*, data exchange is assumed and the satellite can complement the services of BS to serve CUs, thereby remaining the optimized MMF rate at a higher level than that in the *coordinated scheme*. As P_t grows, the benefits of the *cooperative scheme* compared with the *coordinated scheme* decreases. When P_t is sufficiently large, the MMF rates of both schemes will finally converge to the same value due to the fixed satellite transmit power budget P_s. We also investigate the influence of different P_s and N_s setups. Apparently, the larger P_s is, the better MMF rate performance can be achieved. When N_s is increased from 3 to 7, by keeping $\rho = 2$, there will be $K_s = 14$ SUs. We can see that larger N_s leads to lower saturation MMF rates at high P_t region. The larger N_s is, the less transmit power is allocated to each satellite beam. Moreover, each SU will see more inter-beam interference due to the existence of more beams, thus resulting in the performance degradation.

[3]According to the parameters given in Table I and the satellite channel model, the long-term received SNR is calculated to be around 0.67 times the transmit SNR.

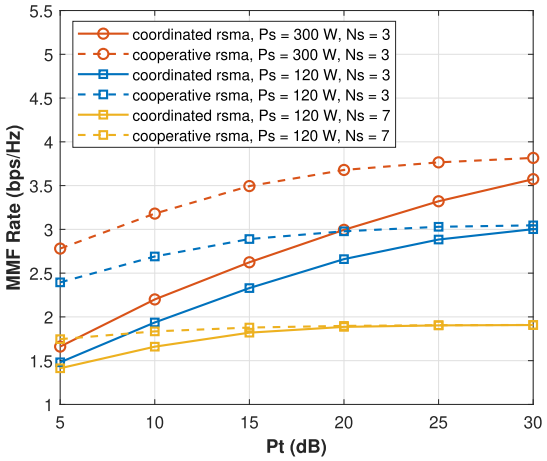

Fig. 3. MMF rate versus P_t with different P_s and N_s. $N_t = 16$, $K_t = 4$, $K_s = \rho N_s$, $\rho = 2$.

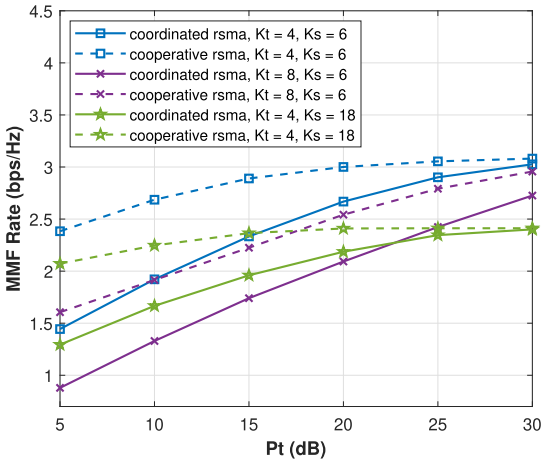

Fig. 4. MMF rate versus P_t with different K_s and K_t. $N_t = 16$, $N_s = 3$, $P_s = 120$W.

Fig. 4 depicts the MMF rates versus P_t with different number of SUs and CUs. When K_t is increased from 4 to 8, the performance will become worse in both *coordinated* and *cooperative scheme* especially at low P_t region, where the CUs take a dominant position of the system's MMF rate. On the other hand, when increasing the number of users per beam ρ

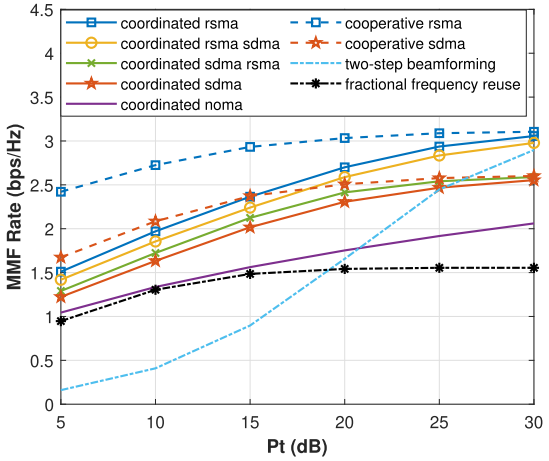

Fig. 5. MMF rate versus P_t with different transmission strategies. $N_t = 16$, $K_t = 4$, $N_s = 3$, $K_s = 6$, $P_s = 120$W.

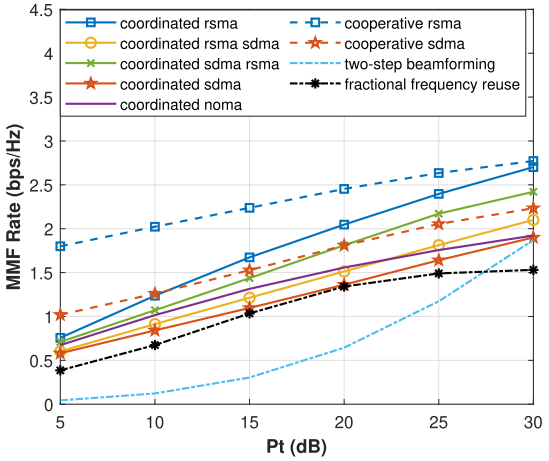

Fig. 6. MMF rate versus P_t for different transmission strategies. $N_t = 4$, $K_t = 4$, $N_s = 3$, $K_s = 6$, $P_s = 120$W.

from 2 to 6, i.e., from $K_s = 6$ to $K_s = 18$, we can still see the performance degradation in both *coordinated* and *cooperative scheme*. The performance degrades much at high P_t region, where the MMF rate is dominated by the satellite sub-system.

In Fig. 5, to investigate the influence of different transmission strategies in STIN, we compare the proposed RSMA-assisted beamforming with baseline strategies including SDMA, NOMA, a two-step beamforming, and fractional frequency reuse. According to the analysis above, here we basically assume $N_s = 3$, $\rho = 2$, $K_s = 6$, $N_t = 16$, $K_t = 4$ for lower computational complexity. Different combinations of transmission strategies are considered in the *coordinated scheme*, e.g., the label "coordinated rsma sdma" means RSMA is used at the satellite while SDMA is used at the BS. It has been shown in [42] that adopting RSMA compared with SDMA in an overloaded system can provide more gains than in an underloaded system. Therefore, in this STIN where the satellite sub-system is always overloaded, and $N_t = 16$ is large enough to support an underloaded cellular sub-system, the performance improvement obtained by using RSMA compared with using SDMA at the satellite is more obvious than at the BS. As a consequence, the "coordinated rsma" successively outperforms "coordinated rsma sdma", "coordinated sdma rsma" and "coordinated sdma". For the "coordinated noma noma", SC-SIC is implemented at both the satellite and BS. The decoding order of NOMA at the satellite is decided by the ascending order of the weakest user's channel strength in each beam. We can observe that the MMF rate achieved by NOMA is the worst compared with RSMA and SDMA. The low performance of NOMA in multi-antenna settings is inline with the observations in [57] and the references therein. As discussed in Fig. 3, *cooperative schemes* can provide higher MMF rates than the corresponding *coordinated schemes*. Thus, the "cooperative rsma" outperforms "coordinated rsma" in Fig. 4, and finally they tend to reach the same MMF rate restricted by the fixed P_s at very large P_t region. Similarly, the "cooperative sdma" outperforms "coordinated sdma". As P_t increases, they converge to the same value which is lower than that of RSMA. For the two-step beamforming, both CSI and data are not exchanged between the satellite and BS. The beamforming for the satellite is at first optimized. Then, the beamforming for the BS is optimized. Since the satellite beamfoming vectors are not jointly designed with the BS beamforming vectors, CUs will see serious interference from the satellite. As P_t grows, the value of minimum rate tends to reach the saturation MMF rate of RSMA-based *coordinated* and *cooperative schemes*. For the scheme of fractional frequency reuse, the satellite and BS operate on different frequency bands. The spectrum cannot be effectively used, therefore resulting in poor MMF rate performance. In [42], it has been demonstrated that the conventional four-color frequency reuse of multibeam satellite systems performs the worst compared with full frequency reuse strategies. Thus, we do not compare with the four-color frequency reuse in this work.

In Fig. 6, the number of BS antennas is reduced to $N_t = 2 \times 2 = 4$, which is not enough to support effective beamforming at the BS so as to eliminate the intra-cell interference and the satellite interference. Compared with Fig. 5 with $N_t = 4 \times 4 = 16$ antennas, the MMF rates of all strategies are suppressed. Specifically, the performance of "coordinated sdma rsma" becomes better than the "coordinated rsma sdma". It implies that when N_t is not sufficient to suppress the intra-cell interference, the gains obtained by using RSMA compared with using SDMA at the BS can become more obvious than at the satellite. We can conclude that the larger N_t is, the better MMF rate performance can be achieved. In other words, as N_t increases, less P_t is required to reach the same MMF rate performance.

Furthermore, we assume imperfect CSI at the GW considering satellite phase uncertainties. Fig. 7 shows the MMF rate performance of the proposed robust joint beamforming in both RSMA-based *coordinated STIN* and *cooperative STIN*. As the variance of phase uncertainty δ^2 increases, the MMF rates of both schemes decrease gradually. From perfect CSIT to imperfect CSIT when $\delta^2 = 5°$, $\delta^2 = 15°$, and the phase-blind scenario, the corresponding MMF rates decrease gradually. The *cooperative STIN* still outperforms *coordinated STIN*. For comparison, we consider the conventional SDMA which performs well amongst the other baseline strategies. From Fig. 8, we can observe that the gaps between perfect CSIT curves and imperfect CSIT curves become larger compared with the RSMA results in Fig. 7. Therefore, RSMA is more

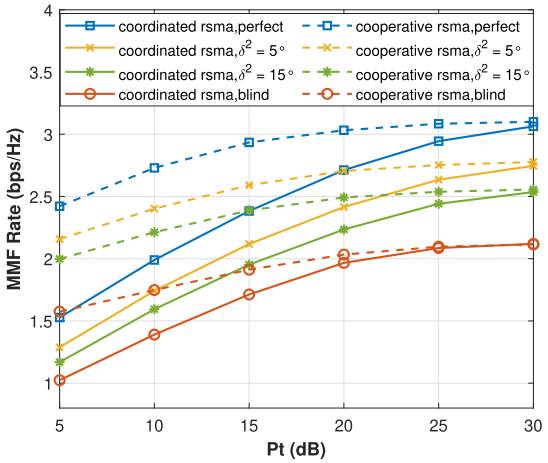

Fig. 7. MMF rate versus P_t with different satellite phase uncertainties. RSMA is adopted at the transmitters. $N_t = 16$, $K_t = 4$, $N_s = 3$, $K_s = 6$, $P_s = 120$W.

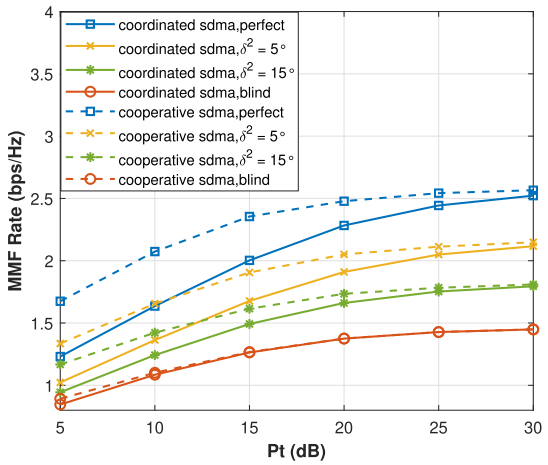

Fig. 8. MMF rate versus P_t with different satellite phase uncertainties. SDMA is adopted at the transmitters. $N_t = 16$, $K_t = 4$, $N_s = 3$, $K_s = 6$, $P_s = 120$W.

robust to the channel phase uncertainty than SDMA due to its more flexible architecture to partially decode the interference and partially treat the interference as noise.

VI. Conclusion

In this work, we investigate the application of RSMA to STIN considering either perfect CSI or imperfect CSI with satellite channel phase uncertainties at the GW. Two RSMA-based STIN schemes are presented, namely the *coordinated scheme* relying on CSI exchange and the *cooperative scheme* relying on both CSI and data exchange at the GW. MMF optimization problems are formulated while satisfying transmit power budgets. To tackle the optimization, two iterative algorithms are respectively proposed. Through simulation results, the superiority of the proposed RSMA-based schemes for STIN is demonstrated compared with various baseline strategies. The robustness of RSMA is verified. In conclusion, RSMA is shown very promising for STIN to manage the interference in and between the satellite and terrestrial subsystems. The study of additional impairments (e.g., limited backhaul, latency on the backhaul, etc) is interesting and is left for future works.

References

[1] Y. Kawamoto, Z. M. Fadlullah, H. Nishiyama, N. Kato, and M. Toyoshima, "Prospects and challenges of context-aware multimedia content delivery in cooperative satellite and terrestrial networks," *IEEE Commun. Mag.*, vol. 52, no. 6, pp. 55–61, Jun. 2014.

[2] H. Zhang, C. Jiang, J. Wang, L. Wang, Y. Ren, and L. Hanzo, "Multicast beamforming optimization in cloud-based heterogeneous terrestrial and satellite networks," *IEEE Trans. Veh. Technol.*, vol. 69, no. 2, pp. 1766–1776, Feb. 2020.

[3] N. U. Hassan, C. Huang, C. Yuen, A. Ahmad, and Y. Zhang, "Dense small satellite networks for modern terrestrial communication systems: Benefits, infrastructure, and technologies," *IEEE Wireless Commun.*, vol. 27, no. 5, pp. 96–103, Oct. 2020.

[4] M. Lin, Z. Lin, W.-P. Zhu, and J.-B. Wang, "Joint beamforming for secure communication in cognitive satellite terrestrial networks," *IEEE J. Sel. Areas Commun.*, vol. 36, no. 5, pp. 1017–1029, May 2018.

[5] S. Vassaki, M. I. Poulakis, A. D. Panagopoulos, and P. Constantinou, "Power allocation in cognitive satellite terrestrial networks with QoS constraints," *IEEE Commun. Lett.*, vol. 17, no. 7, pp. 1344–1347, Jul. 2013.

[6] M. Jia, X. Gu, Q. Guo, W. Xiang, and N. Zhang, "Broadband hybrid satellite-terrestrial communication systems based on cognitive radio toward 5G," *IEEE Wireless Commun.*, vol. 23, no. 6, pp. 96–106, Dec. 2016.

[7] J. P. Choi and C. Joo, "Challenges for efficient and seamless space-terrestrial heterogeneous networks," *IEEE Commun. Mag.*, vol. 53, no. 5, pp. 156–162, May 2015.

[8] S. K. Sharma, S. Chatzinotas, and B. Ottersten, "Transmit beamforming for spectral coexistence of satellite and terrestrial networks," in *Proc. 8th Int. Conf. Cognit. Radio Oriented Wireless Netw.*, Jul. 2013, pp. 275–281.

[9] X. Zhu, C. Jiang, L. Yin, L. Kuang, N. Ge, and J. Lu, "Cooperative multigroup multicast transmission in integrated terrestrial-satellite networks," *IEEE J. Sel. Areas Commun.*, vol. 36, no. 5, pp. 981–992, May 2018.

[10] Y. Zhang, L. Yin, C. Jiang, and Y. Qian, "Joint beamforming design and resource allocation for terrestrial-satellite cooperation system," *IEEE Trans. Commun.*, vol. 68, no. 2, pp. 778–791, Feb. 2020.

[11] Z. Lin, M. Lin, J.-B. Wang, X. Wu, and W.-P. Zhu, "Joint optimization for secure WIPT in satellite-terrestrial integrated networks," in *Proc. IEEE Global Commun. Conf. (GLOBECOM)*, Dec. 2018, pp. 1–6.

[12] J. Li, K. Xue, D. S. L. Wei, J. Liu, and Y. Zhang, "Energy efficiency and traffic offloading optimization in integrated satellite/terrestrial radio access networks," *IEEE Trans. Wireless Commun.*, vol. 19, no. 4, pp. 2367–2381, Apr. 2020.

[13] W. Lu, K. An, and T. Liang, "Robust beamforming design for sum secrecy rate maximization in multibeam satellite systems," *IEEE Trans. Aerosp. Electron. Syst.*, vol. 55, no. 3, pp. 1568–1572, Jun. 2019.

[14] X. Guo, D. Yang, Z. Luo, H. Wang, and J. Kuang, "Robust THP design for energy efficiency of multibeam satellite systems with imperfect CSI," *IEEE Commun. Lett.*, vol. 24, no. 2, pp. 428–432, Feb. 2020.

[15] Z. Lin, M. Lin, J. Ouyang, W.-P. Zhu, A. D. Panagopoulos, and M.-S. Alouini, "Robust secure beamforming for multibeam satellite communication systems," *IEEE Trans. Veh. Technol.*, vol. 68, no. 6, pp. 6202–6206, Jun. 2019.

[16] A. Gharanjik, M. R. B. Shankar, P. D. Arapoglou, M. Bengtsson, and B. Ottersten, "Robust precoding design for multibeam downlink satellite channel with phase uncertainty," in *Proc. IEEE Int. Conf. Acoust., Speech Signal Process. (ICASSP)*, Apr. 2015, pp. 3083–3087.

[17] W. Wang *et al.*, "Resource efficiency optimization for robust beamforming in multi-beam satellite communications," *IEEE Trans. Veh. Technol.*, vol. 70, no. 7, pp. 6958–6968, Jul. 2021.

[18] J. Chu, X. Chen, C. Zhong, and Z. Zhang, "Robust design for NOMA-based multibeam LEO satellite Internet of Things," *IEEE Internet Things J.*, vol. 8, no. 3, pp. 1959–1970, Aug. 2021.

[19] M. Á. Vázquez *et al.*, "Precoding in multibeam satellite communications: Present and future challenges," *IEEE Wireless Commun.*, vol. 23, no. 6, pp. 88–95, Dec. 2016.

[20] L. Yin, B. Clerckx, and Y. Mao, "Rate-splitting multiple access for multi-antenna broadcast channels with statistical CSIT," in *Proc. IEEE Wireless Commun. Netw. Conf. Workshops (WCNCW)*, Mar. 2021, pp. 1–6.

[21] C. Mosquera, N. Noels, T. Ramirez, M. Caus, and A. Pastore, "Space-time rate splitting for the MISO BC with magnitude CSIT," *IEEE Trans. Commun.*, vol. 69, no. 7, pp. 4417–4432, Jul. 2021.

[22] *Second Generation Framing Structure, Channel Coding and Modulation Systems for Broadcasting, Interative Services, News Gathering and Other Broadband Satellite Applications; Part 2: DVB-S2 Extensions (DVB-S2X)*, Standard ETSI EN 302-307-2 V1.1.1, European Broadcasting Union (EBU), Oct. 2014.
[23] B. Clerckx, Y. Mao, R. Schober, and H. V. Poor, "Rate-splitting unifying SDMA, OMA, NOMA, and multicasting in MISO broadcast channel: A simple two-user rate analysis," *IEEE Wireless Commun. Lett.*, vol. 9, no. 3, pp. 349–353, Mar. 2020.
[24] H. Joudeh and B. Clerckx, "Sum-rate maximization for linearly precoded downlink multiuser MISO systems with partial CSIT: A rate-splitting approach," *IEEE Trans. Commun.*, vol. 64, no. 11, pp. 4847–4861, Nov. 2016.
[25] H. Joudeh and B. Clerckx, "Rate-splitting for max-min fair multigroup multicast beamforming in overloaded systems," *IEEE Trans. Wireless Commun.*, vol. 16, no. 11, pp. 7276–7289, Nov. 2017.
[26] Y. Mao, B. Clerckx, and V. O. K. Li, "Rate-splitting multiple access for downlink communication systems: Bridging, generalizing, and outperforming SDMA and NOMA," *EURASIP J. Wireless Commun. Netw.*, vol. 2018, no. 1, p. 133, May 2018.
[27] A. A. Ahmad, H. Dahrouj, A. Chaaban, A. Sezgin, and M. Alouini, "Interference mitigation via rate-splitting and common message decoding in cloud radio access networks," *IEEE Access*, vol. 7, pp. 80350–80365, 2019.
[28] J. Zhang, B. Clerckx, J. Ge, and Y. Mao, "Cooperative rate splitting for MISO broadcast channel with user relaying, and performance benefits over cooperative NOMA," *IEEE Signal Process. Lett.*, vol. 26, no. 11, pp. 1678–1682, Nov. 2019.
[29] C. Hao, Y. Wu, and B. Clerckx, "Rate analysis of two-receiver MISO broadcast channel with finite rate feedback: A rate-splitting approach," *IEEE Trans. Commun.*, vol. 63, no. 9, pp. 3232–3246, Sep. 2015.
[30] H. Joudeh and B. Clerckx, "Robust transmission in downlink multiuser MISO systems: A rate-splitting approach," *IEEE Trans. Signal Process.*, vol. 64, no. 23, pp. 6227–6242, Dec. 2016.
[31] E. Piovano and B. Clerckx, "Optimal DoF region of the K-user MISO BC with partial CSIT," *IEEE Commun. Lett.*, vol. 21, no. 11, pp. 2368–2371, Nov. 2017.
[32] Y. Mao and B. Clerckx, "Beyond dirty paper coding for multi-antenna broadcast channel with partial CSIT: A rate-splitting approach," *IEEE Trans. Commun.*, vol. 68, no. 11, pp. 6775–6791, Nov. 2020.
[33] A. Z. Yalcin, M. Yuksel, and B. Clerckx, "Rate splitting for multi-group multicasting with a common message," *IEEE Trans. Veh. Technol.*, vol. 69, no. 10, pp. 12281–12285, Oct. 2020.
[34] O. Tervo, L.-N. Trant, S. Chatzinotas, B. Ottersten, and M. Juntti, "Multigroup multicast beamforming and antenna selection with rate-splitting in multicell systems," in *Proc. IEEE 19th Int. Workshop Signal Process. Adv. Wireless Commun. (SPAWC)*, Jun. 2018, pp. 1–5.
[35] A. Papazafeiropoulos, B. Clerckx, and T. Ratnarajah, "Rate-splitting to mitigate residual transceiver hardware impairments in massive MIMO systems," *IEEE Trans. Veh. Technol.*, vol. 66, no. 9, pp. 8196–8211, Sep. 2017.
[36] M. Dai and B. Clerckx, "Multiuser millimeter wave beamforming strategies with quantized and statistical CSIT," *IEEE Trans. Wireless Commun.*, vol. 16, no. 11, pp. 7025–7038, Nov. 2017.
[37] Y. Mao, B. Clerckx, and V. O. K. Li, "Rate-splitting for multi-user multi-antenna wireless information and power transfer," in *Proc. IEEE 20th Int. Workshop Signal Process. Adv. Wireless Commun. (SPAWC)*, Jul. 2019, pp. 1–5.
[38] C. Xu, B. Clerckx, S. Chen, Y. Mao, and J. Zhang, "Rate-splitting multiple access for multi-antenna joint communication and radar transmissions," in *Proc. IEEE Int. Conf. Commun. Workshops (ICC Workshops)*, Jun. 2020, pp. 1–6.
[39] M. Caus *et al.*, "Exploratory analysis of superposition coding and rate splitting for multibeam satellite systems," in *Proc. 15th Int. Symp. Wireless Commun. Syst. (ISWCS)*, Aug. 2018, pp. 1–5.
[40] M. Vazquez, M. Caus, and A. Perez-Neira, "Rate splitting for MIMO multibeam satellite systems," in *Proc. 22nd Int. ITG Workshop Smart Antennas*, Mar. 2018, pp. 1–6.
[41] L. Yin and B. Clerckx, "Rate-splitting multiple access for multibeam satellite communications," in *Proc. IEEE Int. Conf. Commun. Workshops (ICC Workshops)*, Jun. 2020, pp. 1–6.
[42] L. Yin and B. Clerckx, "Rate-splitting multiple access for multigroup multicast and multibeam satellite systems," *IEEE Trans. Commun.*, vol. 69, no. 2, pp. 976–990, Feb. 2021.
[43] Z. W. Si, L. Yin, and B. Clerckx, "Rate-splitting multiple access for multigateway multibeam satellite systems with feeder link interference," *IEEE Trans. Commun.*, vol. 70, no. 3, pp. 2147–2162, Mar. 2022.
[44] Z. Lin, M. Lin, T. de Cola, J.-B. Wang, W.-P. Zhu, and J. Cheng, "Supporting IoT with rate-splitting multiple access in satellite and aerial-integrated networks," *IEEE Internet Things J.*, vol. 8, no. 14, pp. 11123–11134, Jul. 2021.
[45] Z. Lin, M. Lin, B. Champagne, W.-P. Zhu, and N. Al-Dhahir, "Secure and energy efficient transmission for RSMA-based cognitive satellite-terrestrial networks," *IEEE Wireless Commun. Lett.*, vol. 10, no. 2, pp. 251–255, Feb. 2021.
[46] D. Christopoulos, S. Chatzinotas, and B. Ottersten, "Multicast multigroup precoding and user scheduling for frame-based satellite communications," *IEEE Trans. Wireless Commun.*, vol. 14, no. 9, pp. 4695–4707, Sep. 2015.
[47] Z. Li, S. Yang, and T. Clessienne, "A general rate splitting scheme for hybrid precoding in mmWave systems," in *Proc. IEEE Int. Conf. Commun. (ICC)*, May 2019, pp. 1–6.
[48] M. Aloisio and P. Angeletti, "Multi-amplifiers architectures for power reconfigurability," in *Proc. IEEE Int. Vac. Electron. Conf.*, May 2007, pp. 1–2.
[49] Y. Mao, B. Clerckx, and V. O. K. Li, "Rate-splitting for multi-antenna non-orthogonal unicast and multicast transmission: Spectral and energy efficiency analysis," *IEEE Trans. Commun.*, vol. 67, no. 12, pp. 8754–8770, Dec. 2019.
[50] O. Tervo, L.-N. Tran, and M. Juntti, "Optimal energy-efficient transmit beamforming for multi-user MISO downlink," *IEEE Trans. Signal Process.*, vol. 63, no. 20, pp. 5574–5588, Oct. 2015.
[51] K.-G. Nguyen, Q.-D. Vu, M. Juntti, and L.-N. Tran, "Distributed solutions for energy efficiency fairness in multicell MISO downlink," *IEEE Trans. Wireless Commun.*, vol. 16, no. 9, pp. 6232–6247, Sep. 2017.
[52] B. R. Marks and G. P. Wright, "A general inner approximation algorithm for nonconvex mathematical programs," *Oper. Res.*, vol. 26, no. 4, pp. 681–683, Aug. 1978.
[53] M. Shao and W.-K. Ma, "A simple way to approximate average robust multiuser MISO transmit optimization under covariance-based CSIT," in *Proc. IEEE Int. Conf. Acoust., Speech Signal Process. (ICASSP)*, Mar. 2017, pp. 3504–3508.
[54] K.-Y. Wang, A. Man-Cho So, T.-H. Chang, W.-K. Ma, and C.-Y. Chi, "Outage constrained robust transmit optimization for multiuser MISO downlinks: Tractable approximations by conic optimization," *IEEE Trans. Signal Process.*, vol. 62, no. 21, pp. 5690–5705, Nov. 2014.
[55] Y. Ye, *Interior Point Algorithms: Theory and Analysis*, vol. 44. Hoboken, NJ, USA: Wiley, 2011.
[56] Z. Lin, M. Lin, J.-B. Wang, T. de Cola, and J. Wang, "Joint beamforming and power allocation for satellite-terrestrial integrated networks with non-orthogonal multiple access," *IEEE J. Sel. Areas Commun.*, vol. 13, no. 3, pp. 657–670, Jun. 2019.
[57] B. Clerckx *et al.*, "Is NOMA efficient in multi-antenna networks? A critical look at next generation multiple access techniques," *IEEE Open J. Commun. Soc.*, vol. 2, pp. 1310–1343, 2021.

Longfei Yin received the B.Eng. degree from the Beijing University of Posts and Telecommunications (BUPT), China, in 2017, and the M.Sc. degree in communications and signal processing from Imperial College London, U.K., in 2018, where she is currently pursuing the Ph.D. degree with the Department of Electrical and Electronic Engineering. Her research interests include wireless communications, signal processing, rate-splitting multiple access, satellite communications, and integrated sensing and communications.

Bruno Clerckx (Fellow, IEEE) is currently a Professor and the Head of the Wireless Communications and Signal Processing Laboratory, and the Deputy Head of the Communications and Signal Processing Group, within the Electrical and Electronic Engineering Department, Imperial College London, London, U.K. He is a f fellow of the IET, and IEEE Communications Society Distinguished Lecturer from 2021 to 2022. He received the prestigious Blondel Medal 2021 in France for exceptional work contributing to the progress of science and electrical and electronic industries, multiple awards from Samsung, and the Best Paper Award 2022 from the European Association for Signal Processing (EURASIP).